# External losses in photoemission from strongly correlated quasi-two-dimensional solids

Hedin, Lars; Lee, J. D.

*Published in:*
Physical Review B

*DOI:*
10.1103/PhysRevB.64.115109

2001

# External losses in photoemission from strongly correlated quasi-two-dimensional solids

L. Hedin[1,2] and J. D. Lee[3,2]
[1]*Department of Physics, University of Lund, Sölvegatan 14A, 22362 Lund, Sweden*
[2]*MPI-FKF, Heisenbergstrasse 1, D-70569 Stuttgart, Germany*
[3]*Department of Physics and Department of Complexity Science and Engineering, University of Tokyo, Bunkyo ku, Tokyo 113, Japan*
(Received 8 January 2001; revised manuscript received 2 May 2001; published 28 August 2001)

Expressions are derived for photoemission, which allow experimental electron energy loss data to be used for estimating losses in photoemission. The derivation builds on new results for dielectric response and mean free paths of strongly correlated systems of two-dimensional layers. Numerical evaluations are made for $Bi_2Sr_2CaCu_2O_8$ (Bi2212) by using a parametrized loss function. The mean free path for Bi2212 is calculated and found to be substantially larger than obtained by Norman *et al.* [Phys. Rev. B **59**, 11 191 (1999)] in a recent paper. The photocurrent is expressed as the convolution of the intrinsic approximation for the current from a specific two-dimensional layer with an effective loss function. This effective loss function is the same as the photocurrent from a core level stripped of the dipole matrix elements. The observed current is the sum of such currents from the first few layers. The correlation within one layer is considered as a purely two-dimensional (2D) problem separate from the embedding three-dimensional (3D) environment. When the contribution to the dielectric response from electrons moving in 3D is taken as diagonal in **q** space, its effect is just to replace bare Coulomb potentials in the (3D) coupling between the 2D layers with dynamically screened ones. The photoelectron from a specific CuO layer is found to excite low-energy acoustic plasmon modes due to the coupling between the CuO layers. These modes give rise to an asymmetric power-law broadening of the photocurrent an isolated two-dimensional layer would have given. We define an asymmetry index where a contribution from a Luttinger line shape is additive to the contribution from our broadening function. Already the loss effect considered here gives broadening comparable to what is observed experimentally. Our theory is not related to the loss mechanism recently discussed by Joynt [R. Joynt, Science **284**, 777 (1999); R. Haslinger and R. Joynt, J. Electron Spectrosc. Relat. Phenom. **117-118**, 31 (2001)] which adds additional broadening beyond what we calculate. A superconductor with a gapped loss function is predicted to have a peak-dip-hump line shape similar to what has been observed, and with the same qualitative behavior as predicted in the recent work by Campuzano *et al.* [Phys. Rev. Lett. **83**, 3709 (1999)].

DOI: 10.1103/PhysRevB.64.115109 PACS number(s): 79.60.−i, 74.25.Gz, 78.20.Bh

## I. INTRODUCTION

Photoemission spectroscopy (PES) is an important tool to understand the electronic structure of strongly correlated quasi-two-dimensional systems such as high-$T_c$ superconductors. Most theoretical work concentrates on two-dimensional (2D) model systems, and when the theoretical results are compared with PES the three dimensionality of the actual experimental samples is only schematically, if at all, taken into account. Further, almost all discussions are based on the sudden approximation (SA), and do not consider extrinsic losses and interference effects. For recent work on strongly correlated systems beyond SA we refer the reader to Refs. 1–4.

We define SA as the bulk one-electron spectral function augmented with dipole matrix elements. This approximation is exact in the high-energy limit for isolated systems such as atoms and molecules. For solids, where the electrons come from a surface region and the mean free path is an important feature, SA is never valid, not even at high energies. Here the correct high-energy limit is a convolution of the sudden approximation and the loss function (SA*LF). SA is particularly valuable when we only look for peak positions such as quasiparticle energies (e.g., for band-structure mapping). There are indications that also quasiparticle line shapes are well represented.[5] When it comes to spectral properties over a more extended energy region, which is important for, e.g., strongly correlated systems, SA can no longer be relied on. For core level photoemission from weakly correlated systems such as metals and valence semiconductors SA*LF correctly describes the satellite intensities only in the keV region, while the asymmetric quasiparticle line shape (in metals) is given correctly by SA already at low energies.[5] For *localized* strongly correlated systems SA is reached rather quickly, say, at 5–10 eV above threshold.[1]

We analyze the three-dimensional (3D) dielectric response of a stack of strongly correlated 2D sheets in the $(x,y)$ plane, embedded in a 3D background. We then assume, as expressed in Eq. (B8), that the response to the total electrostatic potential is given by the sum of a 3D part and a 2D part. With the 3D part depending only on the coordinate difference in 3D, and the 2D part on the difference in 2D, the dielectric function is obtained on a closed form. This closed form allows us to find an approximate relation between the electron energy loss function and the dynamically screened potential $W$. The relation is only approximate since energy loss is related to the diagonal part (in **q**-space) of the dielectric function, while we need the nondiagonal $\mathrm{Im}\,W(z,z',\mathbf{Q},\omega)$ [or equivalently $\mathrm{Im}\,W(q_z,q_z',\mathbf{Q},\omega)$] for the loss problem in photoemission. In PES we need to know $\mathrm{Im}\,W(z,z',\mathbf{Q},\omega)$ in the presence of a surface, while the loss data are obtained from a bulk sample. This calls for addi-

 

tional approximations. Our numerical evaluations concern Bi2212 and are based on a parametrization of the loss function given by Norman *et al.*[4] We, however, include dispersion in the dielectric function, which makes the mean free path much longer. We use atomic units with $|e|=\hbar=m=1$, and thus, e.g., energies are in Hartrees (27.2 eV) and lengths in Bohr radii (0.529 Å).

## II. MEAN FREE PATH

For the interpretation of photoemission from the cuprates the value of the mean free path at energies of about 20 eV, where the experiments usually are done, is very important. In a recent paper by Norman *et al.*[4] very short values of the order 2–3 Å were obtained for Bi2212. Norman *et al.*, however, neglected the **q** dependence in the loss function. In the electron gas case neglect of dispersion makes the mean free path about half the value with dispersion. When we introduce dispersion for Bi2212 we find an even larger effect on the mean free path.

Norman *et al.* used a parametrization of the energy loss data on $Bi_2Sr_2CaCu_2O_8$ (Bi2212) obtained by Nücker *et al.*,[6]

$$\mathrm{Im}\frac{-1}{\varepsilon(\omega)}=\sum_{i=1}^{3} c_i \frac{\omega\Gamma_i\omega_i^2}{(\omega^2-\omega_i^2)^2+\omega^2\Gamma_i^2} \tag{1}$$

with parameters (energies in eV) given below

| $i$ | $c_i$ | $\omega_i$ | $\Gamma_i$ |
|---|---|---|---|
| 1 | 0.164 | 1.1 | 0.7 |
| 2 | 0.476 | 18.5 | 13.6 |
| 3 | 0.345 | 32.8 | 17.0 |

The first peak at about 1 eV is associated with 2D plasmon excitations, while the large double peak comes from essentially 3D excitations since it is similar to what is observed in Cu metal (cf. Ref. 4). The linear rise for small $\omega$ comes from acoustic plasmons (due to the coupling of the 2D plasmons in the different layers), and also to some extent from electron-hole excitations. Phonons and other low-energy excitations cannot be seen in Nücker *et al.*'s[6] data since the broadening is too large (150 meV).

For an electron gas we have the well-known relation between the mean free path $\lambda_{3D}(\varepsilon_k)$ and the inverse dielectric function $\mathrm{Im}\,\varepsilon^{-1}(q,\omega)$,

$$\frac{1}{\lambda_{3D}(\boldsymbol{\varepsilon}_k)}=\frac{2}{\pi k^2}\int_0^\infty\frac{dq}{q}\int_0^{\omega_{\max}}\mathrm{Im}\left[\frac{-1}{\varepsilon(q,\omega)}\right]d\omega, \tag{2}$$

with

$$\boldsymbol{\varepsilon}_k=k^2/2,\quad \omega_{\max}=\min(kq-q^2/2,k^2/2-k_F^2/2).$$

In a solid at lower energies we should use Bloch functions and not plane waves for the scattered electron. However, calculations by Campillo *et al.*[7] show that for copper use of plane waves but with a full-band-structure dielectric function is a reasonable approximation. In our calculations we use Eq. (2) for the two last terms in the Norman *et al.* parametrization. Following Ritchie and Howie[8] and many other authors (cf., e.g, Ref. 9) we introduce dispersion by replacing $\omega_i$ and $c_i$ in Eq. (1) by $\omega_i(q)$ and $c_i(q)$,

$$\omega_i(q)=\omega_i+\frac{q^2}{2},\quad c_i(q)=\frac{c_i\omega_i^2}{\omega_i^2(q)},\quad i=2,3.$$

We have put $k_F=0$ for simplicity, which gives a slight underestimate of the mean free path.

The expression for the mean free path in a layered material is

$$\frac{1}{\lambda_{2D}(\mathbf{k})}=\frac{1}{\pi^2 k}\int_{-\infty}^{\infty}dq_z\int_0^\infty\frac{QdQ}{q_z^2+Q^2}\int_0^{2\pi}d\phi\,\theta(\varepsilon_{\mathbf{k}-\mathbf{q}}-\mu)\times\mathrm{Im}\frac{-1}{\varepsilon(Q;\omega)},$$

where $k_z$ and $\mathbf{K}$ are components perpendicular and parallel to the layers, $\mathbf{k}=(k_z,\mathbf{K})$, $k=|\mathbf{k}|$, $K=|\mathbf{K}|$, etc., and

$$\omega=\varepsilon_{\mathbf{k}}-\varepsilon_{\mathbf{k}-\mathbf{q}}=k_zq_z-q_z^2/2-Q^2/2+KQ\cos\phi.$$

For simplicity we have taken free electron energies. Further considering propagation perpendicular to the layers we have $K=0$, and no dependence on the angle $\phi$ between **K** and **Q**,

$$\frac{1}{\lambda_{2D}(k_z)}=\frac{2}{\pi k}\int_0^k dQ\int_{q_{\min}}^{q_{\max}}\frac{Qdq_z}{q_z^2+Q^2}\mathrm{Im}\frac{-1}{\varepsilon(Q;k_zq_z-q_z^2/2-Q^2/2)}, \tag{3}$$

$$q_{\min}=k-\sqrt{k^2-Q^2},\quad q_{\max}=k+\sqrt{k^2-Q^2}.$$

In Ref. 10 there is a detailed discussion of the 1 eV feature (the first peak). It has a $\mathbf{Q}^2$ dispersion that is a signature of coupled particle holes (plasmons). They also estimate the coefficient theoretically with reasonable results. From Nücker *et al.*[6] it is clear that the first peak, besides dispersing as $Q^2$, quickly broadens when $Q$ increases. For the first term in Eq. (1) we use

$$\omega_1(Q)=\omega_1+\alpha Q^2,\quad \Gamma_1(Q)=\Gamma_1\left(1+\frac{Q^2}{Q_0^2}\right),$$

$$c_1(Q)=\frac{c_1\omega_1^2}{\omega_1^2(Q)},\quad Q_0=0.13\ \text{a.u.},\quad \alpha=0.6.$$

We have put $\mu=0$. With a finite $\mu$, and thus a finite $k_F$ we should replace $\sqrt{k^2-Q^2}$ with $\sqrt{k_F^2-Q^2}$ for $Q<k_F$ in the limits above. Such a replacement makes $1/\lambda_{2D}$ smaller and our approximation thus again slightly underestimates the mean free path.

In Fig. 1 we show results for the inverse mean free paths for the 2D and 3D contributions. It is remarkable that the 2D effects, while peaked at 1.5 eV, extend quite far, out to some 30 eV. The 3D contribution starts dominating at about 10 eV.

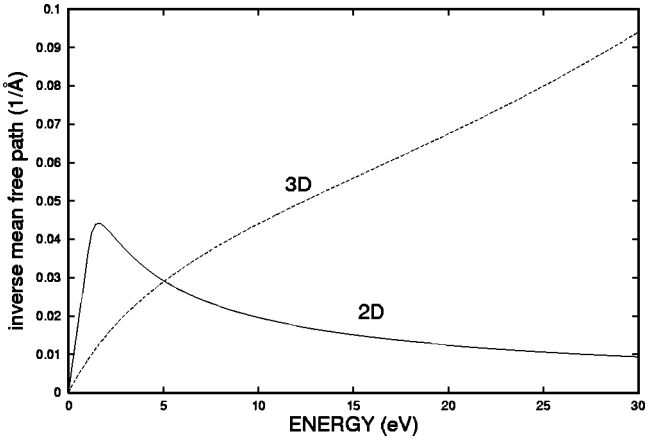


FIG. 1. The contributions to the inverse mean free path $1/\lambda$ from 2D (full drawn) and 3D (dashed) terms in the case of Bi2212.

The mean free path $\lambda$, given by $1/\lambda = 1/\lambda_{2D} + 1/\lambda_{3D}$, is shown in Fig. 2. The maximum in $1/\lambda_{3D}$ is reached at about 100 eV, where the mean free path has its minimum of some 5 Å. It seems to be a universal feature that the minimum mean free path is about 5 Å at an energy about 3–4 times the energy where the loss processes are strongest, as can be seen from tabulations of loss functions[11] and mean free paths.[12] The qualitative behavior of the 2D and 3D contributions in Fig. 1 are similar to what has been obtained in random-phase approximation (RPA) calculations for the layered electron gas.[13] We remark that Norman *et al.* besides the inverse mean free path also calculated the background in PES in the traditional way from the extrinsic losses only, following the common convention to take the background as zero at the bottom of the main band. If we do a similar background calculation the results are very close to Norman *et al.*'s since in such a calculation only the shape and not the strength of the loss function enters. We emphasize that in our treatment of PES later in this paper we include besides the extrinsic losses also the intrinsic ones and the interference terms, which gives a radically different result for small energy losses.

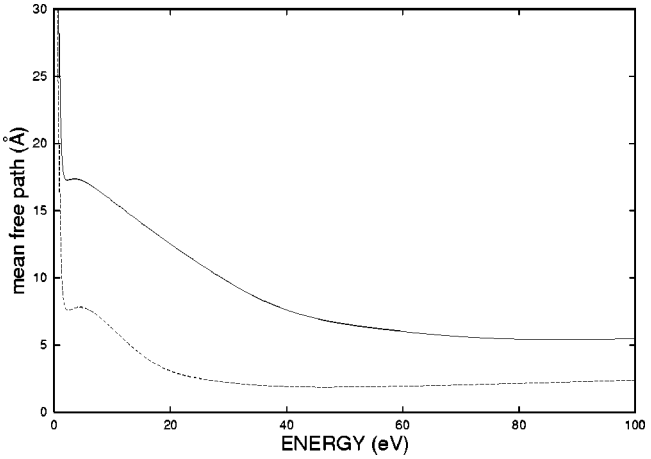


FIG. 2. The full drawn curve gives the mean free path $\lambda$ from our calculations that include dispersion in the dielectric constant, and the dashed curve the results without dispersion given by Norman *et al.*[4]

## III. PHOTOEMISSION

We are interested in photoemission from the CuO layers. The layers are regarded as localized systems embedded in a 3D environment. The crystal surface is taken to be parallel with the layers and in the $(x,y)$ plane. We take the electrons in the 2D layers as separate from the other electrons, and write the state vectors for the initial and final states as

$$|N_B\rangle|N_{2D}\rangle, |N_B^*, s_1\rangle|N_{2D}-1, s_2\rangle|\mathbf{k}\rangle. \tag{4}$$

Here $|N_{2D}\rangle$ is the state vector for the electrons in one particular layer at a distance $z_0$ ($z_0>0$) from the surface (the one from which the photoelectron comes), and $|N_B\rangle$ the state vector for the remaining (bulk) electrons that move in 3D. $|N_{2D}-1,s_2\rangle$ is an excited state $s_2$ of the particular layer, and $|N_B^*,s_1\rangle$ an excited state $s_1$ of the bulk electrons. The star indicates that these electrons move in the presence of a localized hole at $\mathbf{r}=(\mathbf{0},z_0)$, and thus is an eigenfunction of a different Hamiltonian than that for $|N_B\rangle$. Finally, $|\mathbf{k}\rangle$ is the photoelectron state. One may argue that the hole should be extended over the 2D layer rather than sit in one point. However, even in weakly correlated solids correlation effects give rise to satellites corresponding rather to the removal of the electron from a point than from an extended region.[14] For the strongly correlated systems considered here the band is quite narrow and thus the atomic functions building the Bloch functions have small overlaps, which makes our approximation of a localized hole even better. We consider processes when the photo electron energy is high enough that we have reached the sudden limit as far as the excited layer is concerned (about 10 eV according to Ref. 1).

The expression for the PES transition amplitude then becomes[15]

$$\tau(\mathbf{k},s_1,s_2) = \sum_i \langle \mathbf{k}|\langle N_B^*, s_1|\langle N_{2D}-1, s_2| \times \left[1 + V\frac{1}{E-H}\right] c_i|N_{2D}\rangle|N_B\rangle\Delta|i\rangle, \tag{5}$$

where $|i\rangle$ and $|\mathbf{k}\rangle$ are one-electron states. The state $|i\rangle = |\mathbf{K}_i\rangle|\phi_0\rangle$ is the product of a 2D Bloch state $|\mathbf{K}_i\rangle$ with momentum $\mathbf{K}_i$, and the bound state $\phi_0(z)$ for the motion in the $z$ direction, which only will enter as $|\phi_0(z)|^2 = w(z)$. The operator $c_i$ destroys an electron in state "$i$," and $c_i|N_{2D}\rangle$ is regarded as a localized state concerning its influence on the 3D states. The optical transition operator is $\Delta$, and $V$ is the potential for the interaction between the photoelectron and the solid, the potential that causes external losses. Since $V$ contains both operators acting on the photoelectron and on the solid the expectation value $\langle N_B^*, s_1|\cdots V\cdots|N_B\rangle$ is a one-electron operator acting on photoelectron states. The state $\Delta|i\rangle$ generated by optical excitation is considered a photoelectron state. $H$ is the full Hamiltonian including $V$, and $E$ is the total energy

$$E = E(N_{2D}) + E(N_B) + \omega_{phot} = E(N_B^*, s_1) + E(N_{2D}-1, s_2) + \varepsilon_{\mathbf{k}}, \tag{6}$$

where $\omega_{phot}$ is the photon energy and $\varepsilon_{\mathbf{k}}=\mathbf{k}^2/2$ the photoelectron energy. The photocurrent is proportional to

$$J_{\mathbf{k}}(\omega_{phot})\equiv\sum_{s_1 s_2}|\tau(\mathbf{k},s_1,s_2)|^2\delta(\omega_{phot}+E_{s_2}-\omega_{s_1}-\varepsilon_{\mathbf{k}}),$$

with

$$\omega_{s_1}=E(N_B^*,s_1)-E(N_B),$$

$$E_{s_2}=E(N_{2D})-E(N_{2D}-1,s_2).$$

For the Hamiltonian $H$ we take,

$$H=H_{2D}+H_{QB}+h+V,$$

where $H_{2D}$ describes the pertinent 2D layer, $H_{QB}$ the 3D electrons in a quasi-boson representation, $h$ (a one-electron operator) the photoelectron, and $V$ the interaction between the photoelectron and the 3D system (the interaction with the 2D system is neglected since we assume the sudden limit to apply here). Explicitly we have,

$$H_{QB}=\sum_s \omega_s a_s^\dagger a_s - V_h P_h, \quad V_h=\sum_s V_h^s(a_s+a_s^\dagger),$$

$$V=\sum_{s\mathbf{k}\mathbf{k}'} V_{\mathbf{k}\mathbf{k}'}^s c_{\mathbf{k}}^\dagger c_{\mathbf{k}'}(a_s+a_s^\dagger), \quad V_{\mathbf{k}\mathbf{k}'}^s=\langle\mathbf{k}|V^s|\mathbf{k}'\rangle,$$

$$V_h^s=V^s(\mathbf{0},z_0).$$

$P_h$ is a projection operator that gives 1 for states with a hole in the 2D system, and 0 otherwise, and $V_h$ is the potential from the hole in the 2D system. The functions $V^s(\mathbf{r})$ are fluctuation potentials, discussed at length in Refs. 5 and 15.

Say that we somehow can calculate the photocurrent $J_{\mathbf{k}}^{2D}(z_0,\omega_{phot})$ from one isolated two-dimensional layer at a distance $z_0$ from the surface, and want to estimate the current from this layer when a set of such layers together with additional electrons of 3D character form a three-dimensional crystal. We have to account for the shake up in the 3D surrounding of the layer as well as the losses the photoelectron can have on its way out to the surface. In Appendix A we show that the photocurrent then can be written as a convolution between the 2D current $J_{\mathbf{k}}^{2D}(z_0,\omega)$ and an effective broadening function $P_{\mathbf{k}}(z_0,\omega)$ [Eqs. (A4) and (A5)],

$$J_{\mathbf{k}}(z_0,\omega_{phot})=\int J_{\mathbf{k}}^{2D}(z_0,\omega')P_{\mathbf{k}}(z_0,\omega_{phot}-\omega')d\omega'. \tag{7}$$

A delta function peak $\delta(\omega-\varepsilon_0-\varepsilon_{\mathbf{k}})$ in $J_{\mathbf{k}}^{2D}(z_0,\omega)$ will hence give a contribution $P_{\mathbf{k}}(z_0,\omega_{phot}-\varepsilon_0-\varepsilon_{\mathbf{k}})$ to the photocurrent. In core-electron photoemission we have a similar expression with $J_{\mathbf{k}}^{2D}(z_0,\omega)$ replaced by the expression for the current from a core level in an isolated ion (essentially a delta function).

The common energy distribution curve experiment gives the current for fixed photon energy $\omega_{phot}$ as a function of the electron energy $\varepsilon_{\mathbf{k}}$ for a given direction of $\mathbf{k}$ (or $\mathbf{K}$, where $\mathbf{k}=k_z\hat{z}+\mathbf{K}$). We are thus interested in $P_{\mathbf{k}}(z_0,\omega_{phot}-\varepsilon_0-\varepsilon_{\mathbf{k}})$ as a function of $\varepsilon_{\mathbf{k}}$ in the range $\omega_{phot}-\varepsilon_0>\varepsilon_{\mathbf{k}}>0$. Since $P_{\mathbf{k}}(z_0,\omega)$ varies fairly slowly with $\mathbf{k}$ for fixed $\omega$, $P_{\mathbf{k}}(z_0,\omega)$ as a function of $\omega$ for fixed $\mathbf{k}$ describes the photoemission (in a limited energy range). We will mainly discuss the properties of $P_{\mathbf{k}}(z_0,\omega)$ as a function of $\omega$ for fixed $\mathbf{k}$.

The effective broadening function to second order in $V^s$ is found to be (Appendix A),

$$P_{\mathbf{k}}(z_0,\omega)=e^{-z_0/\lambda-a}\left[\delta(\omega)+\frac{\alpha(\mathbf{k},z_0;\omega)}{\omega}\right], \tag{8}$$

where

$$\frac{\alpha(\mathbf{k},z_0;\omega)}{\omega}=\sum_s\left|\int_0^{z_0} f(\mathbf{k},\mathbf{Q},\omega,z_0;z)V(q_z,\mathbf{Q},z)dz\right|^2\delta(\omega-\omega_s), \tag{9}$$

$$f(\mathbf{k},\mathbf{Q},\omega,z_0;z)=-\frac{\delta(z-z_0)}{\omega}+\frac{e^{i(\kappa-\tilde{k}_z)z_0}}{i\kappa}e^{i\tilde{k}_z z}e^{-i\kappa z}. \tag{10}$$

This expression is the same as in Eqs. (26) and (27) for the core electron current in Ref. 5. The function $V(q_z,\mathbf{Q},z)$ in Eq. (9) is the fluctuation potential giving the coupling between the photoelectron and a density fluctuation $s=(q_z,\mathbf{Q})$ with energy $\omega_s$. In $f(z)$ the first term gives the intrinsic or shake-up contribution to the amplitude, while the second term gives the contribution from losses when the electron propagates from the layer at $z_0>0$ to the surface at $z=0$. The quantities $\kappa$ and $\tilde{k}_z$ are the (complex) momenta in the $z$ direction of the photoelectron when inside the solid before and after it excited the density fluctuation $s$ having parallel momentum $\mathbf{Q}$. The photoelectron momentum outside the solid is $k_z\hat{z}+\mathbf{K}$ and its energy $\varepsilon_{\mathbf{k}}=(k_z^2+\mathbf{K}^2)/2$. Further, $V_0$ is the (negative) inner potential, and $\Gamma_1$ and $\Gamma_2$ are the dampings before and after emitting the excitation $s$. It is easy to derive expressions where the plane waves $e^{ikz}$ and $e^{-i\kappa z}$ are replaced by (damped) Bloch functions, and can find expressions where the band structure also is present in the lateral motion.

Since $P_{\mathbf{k}}(\omega)$ is quadratic in the fluctuation potentials $V^s$, we can relate it to the dynamically screened potential $W$. For the imaginary part of $W$ we have [cf. Eq. (49) in Ref. 5],

$$\mathrm{Im}\,W(z,z';\mathbf{R},\mathbf{R}';\omega)=-\pi\sum_s V^s(\mathbf{r})V^s(\mathbf{r}')\delta(\omega-\omega_s).$$

With $V^s(\mathbf{r})=e^{i\mathbf{Q}\mathbf{R}}V(q_z,\mathbf{Q},z)$

$$\mathrm{Im}\,W(z,z';\mathbf{Q};\omega)=-\pi A\sum_{q_z} V(q_z,\mathbf{Q},z)V(q_z,\mathbf{Q},z')\delta(\omega-\omega_s),$$

where $A$ is the normalization area of the planes. In an exact treatment the $V(q_z,\mathbf{Q},z)$ can be chosen real, and we see that $\mathrm{Im}\,W(z,z';\mathbf{Q};\omega)$ is symmetric in $z$ and $z'$. Comparison with Eqs. (8) and (9) shows that

$$\frac{\alpha(\mathbf{k},z_0;\omega)}{\omega}=-\frac{1}{\pi A}\sum_{\mathbf{Q}}\int_0^{z_0} f(\mathbf{k},\mathbf{Q},\omega,z_0;z)\times \mathrm{Im}\,W(z,z';\mathbf{Q};\omega)f(\mathbf{k},\mathbf{Q},\omega,z_0;z')^* dz dz'.$$

To simplify the calculations we relate $\mathrm{Im}\,W$ to the measured loss function. The loss function, however, is connected with losses in the bulk, and we also have to find an approximate relation between $\mathrm{Im}\,W^{bulk}$ and $\mathrm{Im}\,W^{surf}$. This was done in Ref. 5 by using the Inglesfield simplified expression for the fluctuation potential,

$$\mathrm{Im}\,W_{3D}^{surf}(z,z',\mathbf{Q},\omega)=\frac{1}{2\pi}\int_0^{\infty} F(q_z,Q,z)F(q_z,Q,z')\times \mathrm{Im}\,W_{3D}^{bulk}(q_z,\mathbf{Q},\omega)dq_z,$$

where

$$F(q_z,Q,z)=2[\cos(q_z z+\phi_{\mathbf{q}})-\cos\phi_{\mathbf{q}} e^{-Qz}]\theta(z),$$

$$\phi_{\mathbf{q}}=\arctan\frac{q_z}{Q}.$$

This means that for the strength of the coupling we keep the bulk expression, while for the spacial part we have a bulk function (here plane wave) that is modified to be zero at the surface. The relation to the loss function is

$$\mathrm{Im}\,W_{3D}^{bulk}(q_z,\mathbf{Q},\omega)=v(q_z,Q)\mathrm{Im}\frac{-1}{\varepsilon^{3D}(q_z;\mathbf{Q};\omega)}.$$

For 2D excitations we can do a similar modification of the bulk fluctuation potential to make it zero at the surface. When we take $w(q_z)=1$ we have (see Appendix B)

$$\mathrm{Im}\,W_{2D}^{surf}(z,z';\mathbf{Q};\omega)=\frac{1}{2\pi}\int_0^{\pi/c} V^r(q_z,\mathbf{Q},z-z_0)V^r(q_z,\mathbf{Q},z'-z_0)\times \mathrm{Im}\frac{\chi_0(q_z;\mathbf{Q};\omega)}{c}dq_z$$

for the contribution from the layer at $z_0$, where $\mathrm{Im}\,\chi(q;\mathbf{Q};\omega)$ is related to the loss function by

$$\mathrm{Im}\frac{\chi_0(q_z;\mathbf{Q};\omega)}{c}=\frac{1}{2v(q_z,Q)}\mathrm{Im}\frac{-1}{\varepsilon^{2D}(q_z;\mathbf{Q};\omega)},$$

and $V^r(q_z,\mathbf{Q},z)$ is the fluctuation potential,

$$V^r(q_z,\mathbf{Q},z)=2\,\mathrm{Re}[V^p(q_z,Q;z)\exp\{-iq_z z+i\phi(z_0)\}]. \tag{11}$$

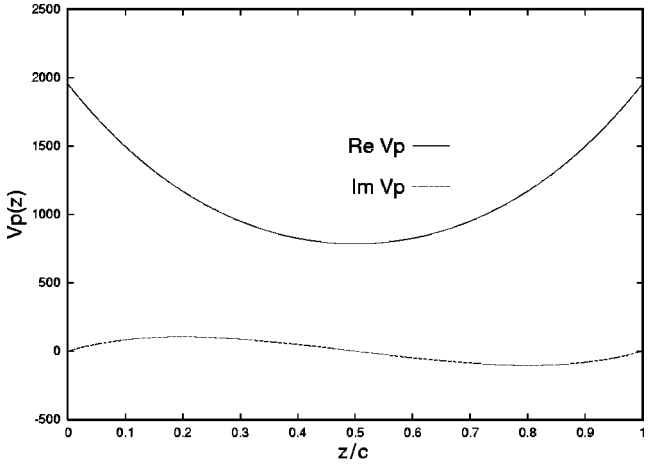


FIG. 3. The periodic functions $\mathrm{Re}\,V^p(z)$ and $\mathrm{Im}\,V^p(z)$ for $z/c$ in the interval (0,1), where $c$ is the lattice constant and $V^p$ is defined in Eq. (12). We have taken some typical values, $q=0.03$ and $Q=0.1$ (for Bi2212 $c=29.1$ and $a=10.2$, which gives $\pi/c=0.11$ and $\pi/a=0.31$).

Here $V^p(q_z,Q;z)$ is a well-known periodic potential [$V^p=\exp(iq_z z)V$, with $V$ defined in Eq. (B7)]

$$V^p(q_z,Q;z)=\sum_G v(q_z+G,Q)w(q_z+G)e^{-iGz}=\frac{2\pi c e^{iq_z z}}{Q}\frac{\sinh Q(c-z)+e^{-iq_z c}\sinh Qz}{\cosh Qc-\cos q_z c}. \tag{12}$$

The explicit expression follows when the form factor $w(q_z)$ (cf. Appendix B) is taken as 1, and is valid only for $0<z<c$. The phase $\phi(z_0)$ in Eq. (11) is chosen to make $V^r$ zero at the surface, $V^r(q_z,\mathbf{Q},z_0)=0$.

In Fig. 3 we plot $\mathrm{Re}\,V^p(z)$ and $\mathrm{Im}\,V^p(z)$ for some typical values of $q_z$ and $Q$, and in Fig. 4 we show $V^r(z)$ for the same

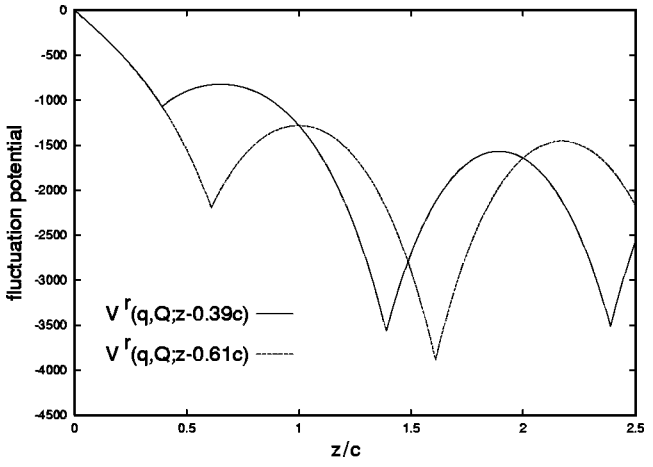


FIG. 4. The fluctuation potential $V^r(q,Q;z-z_i)$ in Eq. (11) for $z/c$ in the interval (0,2.5) and for $z_i=0.39c$ and $0.61c$, the distances from the surface of the first two CuO layers. The potentials are zero at the surface and the cusps come at CuO layers. The maximum possible value of $|V^r|$ is $2V^p(0)$.

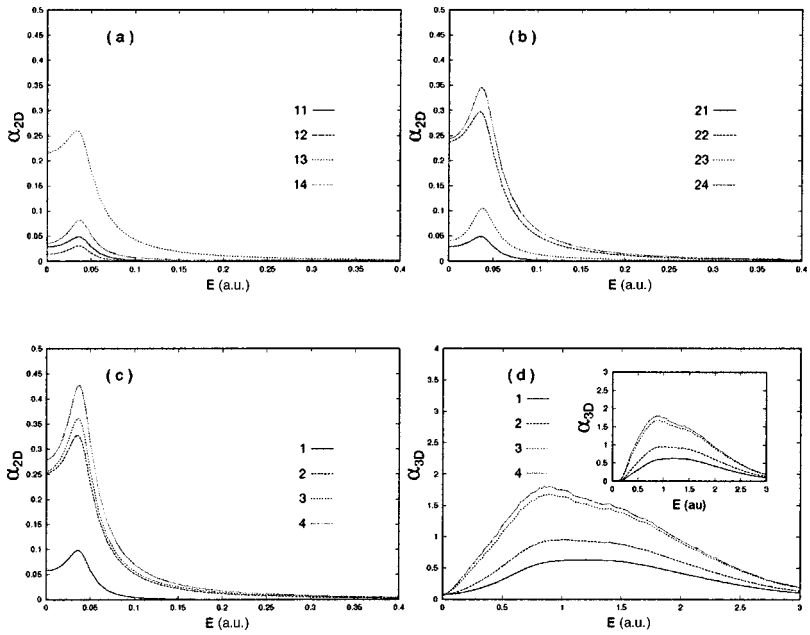


FIG. 5. Results for $\alpha_{2D}(\omega)$ and $\alpha_{3D}(\omega)$ [cf. Eqs. (17) and (18)]. The parameter values are obtained from energy loss data for Bi2212. The curves in Figs. 5(a),(b) give contributions to $\alpha_{2D}(\omega)$. The symbol *mn* refers to a contribution when the fluctuation potential is centered at layer $m$ (and $m+2$, $m+4$, etc.) and the photocurrent comes from layer $n$. Thus the dashed curve in Fig. 5(a) ($m=1$, $n=2$) refers to a contribution from the fluctuation potential centered on the layer closest to the surface when the photocurrent comes from the second layer. Figure 5(c) shows the total contributions to $\alpha_{2D}(\omega)$ when the current comes from layers 1 to 4, and Fig. 5(d) shows the corresponding contributions to $\alpha_{3D}(\omega)$. The curves in the inset are *ad hoc* adjusted to take out the unphysical low-energy part coming from a schematic parametrization. The photon energy is 1 a.u.

parameter values. The sharp peak with a singular derivative in $\mathrm{Re}\,V^p(z)$ at $z=0$ is smoothened if we take $w(q)\neq 1$. For a typical binding energy of 3 eV and an exponential wave function, we have $w(q_z)=a^2/(a^2+q_z^2)$, with $a=0.9$. Typical values of $q_z$ and $Q$ are $\pi/c$ and $\pi/a$. The lattice parameters for Bi2212 are $c=29.1$ and $a=10.22$, which makes $\pi/c=0.11$ and $\pi/a=0.31$.[16] We can also compare with the cutoff parameter for the collective excitations in Bi2212 discussed in the section on mean free path, $Q_0=0.13$. Thus $a$ is substantially larger than $q$ and $Q$, and it is hence reasonable to take $w(q_z)=1$. We note that the values of $\mathrm{Re}\,V^r(z)$ at the first two Cu layers are substantially smaller than the maximum value of $\mathrm{Re}\,2V^p(z)$. An approximation with bulk potentials cut at the surface clearly can give very large and spurious effects unless we go to so extremely high energies that the mean free path becomes much larger than the lattice parameter $c$.

When there are no low-energy excitations, like for an insulator or for a metal when the electron-hole excitations are neglected and only the plasmons are kept, the overlap between the initial ground state and the completely relaxed ground state in the presence of a localized hole potential is finite. In a quasi-boson treatment we have

$$|\langle N_B^*,0|N_B,0\rangle|^2=e^{-a},\quad a=\sum_s\left|\frac{V^s(z_0)}{\omega_s}\right|^2.$$

A partial summation of the perturbation expansion in $V^s$ (or a cumulant expansion) gives[5]

$$P_{\mathbf{k}}(z_0,\omega)=\int\frac{dt}{2\pi}e^{-i\omega t}\exp\left(\int\alpha(\mathbf{k},z_0;\omega')\frac{e^{i\omega' t}-1}{\omega'}d\omega'\right). \tag{13}$$

This expression correctly reproduces the edge singularity, $1/\omega^{1-\alpha(\mathbf{k},z_0;0)}$, and also gives the second-order satellite term in Eq. (8). In the high-energy limit and the plasmon pole approximation (the electron-hole part is then not included) it can be shown analytically that[5]

$$\int\frac{\alpha(\mathbf{k},z_0;\omega)}{\omega}d\omega=a+z_0/\lambda, \tag{14}$$

and Eq. (13) thus also gives the correct prefactor in this limit.

With an electron-hole continuum, Eq. (14) no longer can hold since the integral diverges. We then split $\alpha(\mathbf{k},\omega_{phot};\omega)$ in a 2D part from the excitations in the layers, and a 3D part from the remaining excitations, $\alpha=\alpha_{2D}+\alpha_{3D}$. The 3D contributions in Eq. (1) have been smoothly deformed to be zero for $\omega<\omega_{th}=0.1$ since the metallic excitations come from the layers. To give a good representation of the experimental loss function this deformation should be compensated by a small increase in the 2D term, but this is a minor effect that we have omitted. Now the integral $\int_{\omega_{th}}^{\infty}d\omega\alpha_{3D}(\mathbf{k},\omega_{phot};\omega)/\omega$ converges, and we have checked numerically that in the high-energy limit

$$\int_{\omega_{th}}^{\infty}\frac{\alpha_{3D}(\mathbf{k},z_0;\omega)}{\omega}d\omega=a_{3D}^{intr}+z_0/\lambda, \tag{15}$$

where $a_{3D}^{intr}$ contains only the intrinsic part,

$$a_{3D}^{intr}=\int_{\omega_{th}}^{\infty}\sum_s|V_{3D}^s(z_0)|^2\delta(\omega-\omega_s)\frac{d\omega}{\omega^2}.$$

The approach to the high-energy limit is quite slow (of the order of keV), and in our estimates for Bi2212 we adopt the expression

$$P_{\mathbf{k}}(\omega)=\exp(-z_0/\lambda-a_{3D}^{intr})\int\frac{dt}{2\pi}e^{-i\omega t}\times\exp\left[\int_0^\infty\alpha_{2D}(\mathbf{k},z_0;\omega')\frac{e^{i\omega' t}-1}{\omega'}d\omega'+\int_{\omega_{th}}^\infty\alpha_{3D}(\mathbf{k},z_0;\omega')\frac{e^{i\omega' t}}{\omega'}d\omega'\right]. \quad (16)$$

Equation (16) guarantees the correct dependence on the distance $z_0$ to the layer. While $\exp(-a_{3D}^{intr})$ may not give an accurate scale factor, this is of minor importance since it does not affect the ratio between the threshold peak and the satellite structure. The $\alpha_{3D}^{intr}$ values depend only weakly on $z_0$, and for the first four layers the values are 0.243, 0.252, 0.260, and 0.261. Collecting our results we have

$$\alpha_{2D}(\mathbf{k},z_0;\omega)=\frac{-\omega}{\pi(2\pi)^3}\int_0^{\pi/c}dq_z\int d\mathbf{Q}\times\left|\int_0^{z_0}f(z)V^r(q_z,\mathbf{Q},z)dz\right|^2\mathrm{Im}\,\chi(q_z,\mathbf{Q},\omega), \quad (17)$$

$$\alpha_{3D}(\mathbf{k},z_0;\omega)=\frac{-\omega}{\pi(2\pi)^3}\int_0^{\infty}dq_z\int d\mathbf{Q}\times\left|\int_0^{z_0}f(z)F(q_z,Q,z)dz\right|^2\mathrm{Im}\,W_b(q_z,\mathbf{Q},\omega). \quad (18)$$

In Fig. 5 we plot results for different contributions to the $\alpha$ functions in Eq. (16). The general shape of the $\alpha_{2D}(\omega)$ functions is similar to the electron gas case with a flat portion for small $\omega$ followed by a plasmon peak (cf. Ref. 17, pp. 663–667). However, the magnitudes are different, $\alpha_{2D}(0)$ is fairly large (0.25–0.30) compared to metals while the plasmon peak is much smaller and broader. When we change the parametrization to make the 3D terms start at 0.1 a.u. the $\alpha_{2D}(0)$ values will increase by some 10%. The $\alpha_{2D}$ functions have only a weak dependence on photon energy, while the $\alpha_{3D}$ curves have a much larger dependence. All curves in Fig. 5 are for the same photon energy of 1 a.u.

The left part of Fig. 6 shows the dominance of the intrinsic contributions to $\alpha_{2D}$. As expected the contributions from the extrinsic terms are larger for the layers further away from the surface. The right part shows the approach towards the bulk value of the intrinsic contributions for $\alpha_{2D}$ and $\alpha_{3D}$. This approach is considerably slower in the 2D case as might be expected from the behavior of the fluctuation potentials (cf. Fig. 4). Comparing the intrinsic $\alpha_{3D}$ in Fig. 6 with the full $\alpha_{3D}$ in Fig. 5, we see that in the 3D case the extrinsic effects dominate. The difference $\alpha_{3D}^{full}-\alpha_{3D}^{intr}$ is roughly proportional to $z_0$ that follows the trend in the high-energy sum rule, Eq. (15). In Fig. 7 the contributions from $P_k(z_0,\omega)$ in Eq. (16) from the first four CuO layers are shown. It is clear that most of the asymmetry comes from the layers in the first

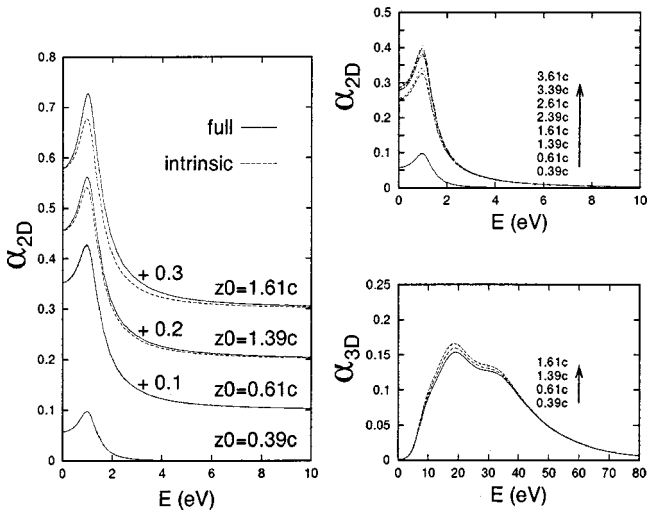


FIG. 6. The left part shows a comparison of $\alpha_{2D}(\omega)$ for the pure intrinsic case with the full expression including the extrinsic amplitude. The right part shows how the pure intrinsic contributions to $\alpha_{2D}(\omega)$ and $\alpha_{3D}(\omega)$ converge towards their bulk values. The photon energy is 1 a.u.

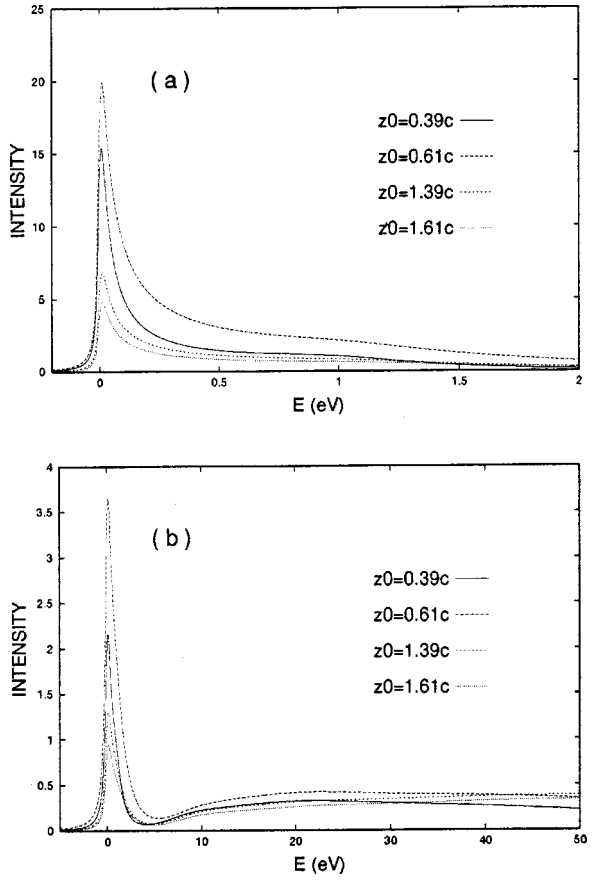


FIG. 7. The effective loss function $P_{\mathbf{k}}(\omega)$ including both 2D and 3D contributions [cf. Eq. (16)]. The contributions from the different layers are displayed separately. The curves are convoluted with Lorentzians, in Fig. 7(a) with $\Gamma=10$ meV, and in Fig. 7(b) with $\Gamma=300$ meV.

unit cell. The alpha function for the first copper layer is quite small (Fig. 6), but when the mean free path effects are taken into account, Fig. 7 shows that the broadening contributions from the first and second layers are comparable. Figure 7(b) shows an extended energy region to illustrate the relative importance of the 2D and 3D contributions. The integral effect of the 3D contributions is much larger, but the peaks in the loss function are smoothened out and the 3D contribution is featureless. At higher energies we of course also have contributions to the photocurrent from other states than the quasi-2D ones in the Copper layers discussed in this paper.

We now give a qualitative discussion of the effective broadening function $P_{\mathbf{k}}(\omega)$ in Eq. (16). Since the 2D and 3D contributions add in an exponent we can write $P_{\mathbf{k}}(\omega)$ as a convolution,

$$P_{\mathbf{k}}(z_0,\omega)$$

$$=\exp(-z_0/\lambda-a_{3D}^{intr})\int P_{\mathbf{k}}^{2D}(\omega-\omega')P_{\mathbf{k}}^{3D}(\omega')d\omega'.$$

For $P_{\mathbf{k}}^{3D}$ we make a Taylor expansion, and keep only the first term, $P_{\mathbf{k}}^{3D}(\omega)=\delta(\omega)+\alpha_{3D}(\omega)/\omega$. We have then omitted the multiple quasi-boson excitations starting at $\omega=2\omega_{th}$. Since $P_{\mathbf{k}}^{2D}$ is normalized to unity, and consists of a peak that is sharp compared to $\alpha_{3D}$, we can write

$$P_{\mathbf{k}}(z_0,\omega)$$

$$\simeq\exp(-z_0/\lambda-a_{3D}^{intr})\left[P_{\mathbf{k}}^{2D}(z_0,\omega)+\frac{\alpha_{3D}(\mathbf{k},z_0;\omega)}{\omega}\right].$$

To numerically evaluate $P_{\mathbf{k}}^{2D}(\omega)$ we used the integral equation $\omega P_{\mathbf{k}}^{2D}(\omega)=\int_0^{\omega}d\omega'\,\alpha_{2D}(\omega')P_{\mathbf{k}}^{2D}(\omega-\omega')$ which is easier then to evaluate the exponential expression in Eq. (16). If we approximate $\alpha_{2D}(\omega)$ by a rectangular function, $\alpha_{2D}(\omega)=\alpha_0\theta(\omega_0-\omega)$, and broaden with a Lorentzian of width $\Gamma$ (full width at half maximum $=2\Gamma$), we have for $\omega<\omega_0$ the Doniach-Sunjic expression,[18]

$$P_{\mathbf{k}}^{2D}(\omega)=C(\alpha_0)\frac{\cos[\pi\alpha_0/2-(1-\alpha_0)\arctan(\omega/\Gamma)]}{[1+(\omega/\Gamma)^2]^{(1-\alpha_0)/2}},$$

$$C(\alpha_0)=\frac{e^{-\gamma\alpha_0}}{(\alpha_0-1)!\,\omega_0^{\alpha_0}\Gamma^{1-\alpha_0}\sin[\pi\alpha_0]}, \qquad (19)$$

where $\gamma=0.577$ is the Euler constant. The coefficient $C(\alpha_0)$ in Eq. (19) was derived in Ref. 17 [see Eq. (162)]. For $\omega>\omega_0$ $P_{\mathbf{k}}^{2D}(\omega)$ only has a weak tail with less than 10% of the norm (for $\alpha_0<0.4$). Let $\omega_{\max}$ be the $\omega$ value for which $P_{\mathbf{k}}^{2D}(\omega)$ has its maximum, and $\omega_1$ and $\omega_2$ the values where it takes half its maximum value. We define an asymmetry index $\gamma_{as}(\alpha_0)=(\omega_2-\omega_{\max})/(\omega_{\max}-\omega_1)$. An approximate expression for $\gamma_{as}$ is

$$\gamma_{as}(\alpha_0)=\frac{\omega_2-\omega_{\max}}{\omega_{\max}-\omega_1}=1+0.79\alpha_0+14.54\alpha_0^2. \qquad (20)$$

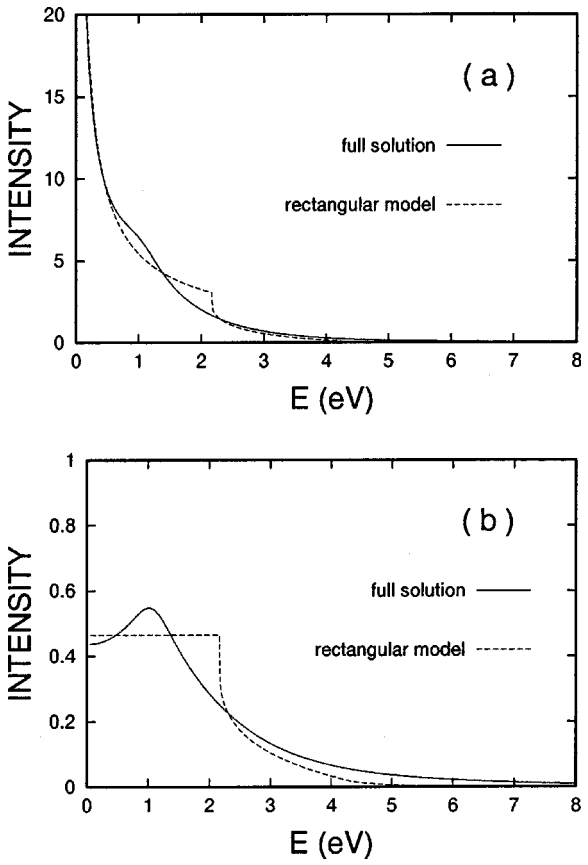


FIG. 8. The effective loss function $P_{\mathbf{k}}^{2D}(\omega)$ obtained with only the 2D contribution from the second layer. The full drawn curve in Fig. 8(a) shows the full solution obtained with the ''2'' curve in Fig. 5(c), while the dashed curve shows the result using the rectangular approximation for $\alpha_{2D}(\omega)$ with $\omega_0=0.08$ and $\alpha_0=0.255$ [see text at Eq. (19)]. In Fig. 8(b) we show $\omega^{[1-\alpha(0)]}P_{\mathbf{k}}(\omega)$. The photon energy is 1 a.u.

$P_{\mathbf{k}}^{2D}(\omega)$ is the function that broadens a $\delta$-function peak in $J_{\mathbf{k}}^{2D}(\omega)$. If $J_{\mathbf{k}}^{2D}(\omega)$ has a Doniach-Sunjic singular shape the broadening with $P_{\mathbf{k}}^{2D}(\omega)$ still gives Eq. (19) but with an $\alpha_0$ that is the sum of the alphas in $J_{\mathbf{k}}^{2D}$ and in $P_{\mathbf{k}}^{2D}(\omega)$. This is so because the time transform of a power-law singularity $\omega^{-(1-\alpha_0)}$ is $t^{-\alpha_0}$, and a convolution in frequency space is a product in time space.

The $\alpha_{2D}$ functions in Fig. 5 show clear peaks due to the plasmon excitations. The peaks are, however, not strong enough to give more than a small bump in the $P_{\mathbf{k}}^{2D}$ functions. This is illustrated in Fig. 8(a) that shows the full $P_{\mathbf{k}}^{2D}$ curve and the rectangular approximation in Eq. (19) using $\alpha_0=0.255$ and $\omega_0=0.08$ a.u.$=2177$ meV. In Fig. 8(b) the rectangular approximation is illustrated by taking out the singularity and plotting $P_{\mathbf{k}}^{2D}(\omega)\omega^{[1-\alpha_{2D}(0)]}$. The simple rectangular approximation without plasmon peak should be useful as a guide when other broadening effects are at work. In Fig. 9 we show the sum for the first four layers of the 2D contributions $\exp(-z_0/\lambda-a_{3D}^{intr})P_{\mathbf{k}}^{2D}(\omega)$ broadened with different Lorentzians. The 3D terms are not included except for the (all important) mean free path factor. In the first three panels with a limited energy region (up to 500 meV) we have used

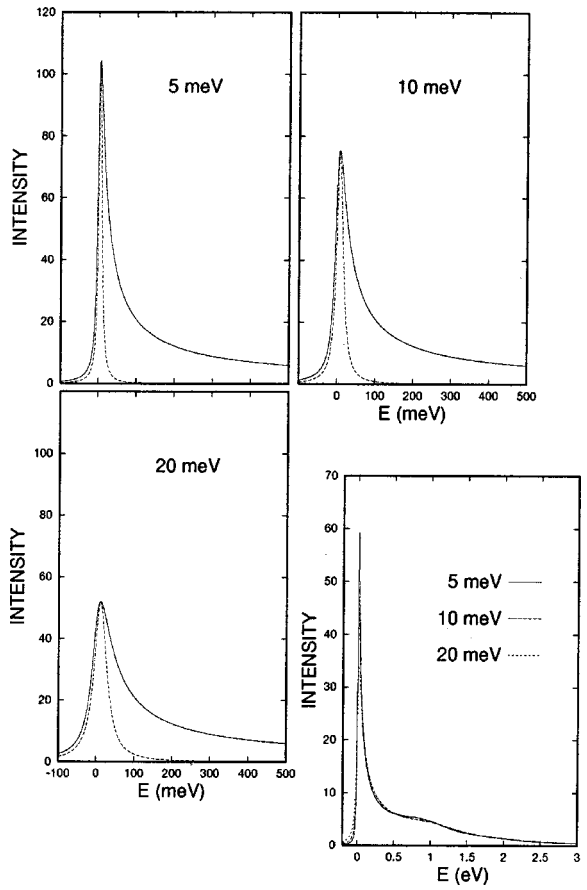


FIG. 9. The effective loss function $P_{\mathbf{k}}(\omega)$ convoluted with Lorentzians of different widths $\Gamma$ (5, 10, and 20 meV). All the 2D contributions $P_{\mathbf{k}}^{2D}(\omega)$ in Eq. (19) from the first four layers are summed weighted with $\exp(-z_0/\lambda-\alpha_{3D}^{intr})$. The 3D terms are not included. In the first three panels we have used the rectangular approximation, while in the last panel the full evaluation from Eq. (16) was done. Also the Lorentzians are shown. The photon energy is 1 a.u.

the rectangular approximation for the different $\alpha_{2D}$ contributions. In the last panel with a larger energy range the full evaluation from Eq. (16) was done since it is superior to the rectangular model for energies above 0.5 eV (see Fig. 8). The numerical accuracy at the peak is, however, lower in the full calculation. Also the Lorentzians are shown to ease the estimate of the size of the asymmetries. It is clear that we have a sizeable line asymmetry, and also a long tail extending over several eV. The artificial step in the rectangular approximation at about 3 eV (Fig. 8) is of little consequence since the intensity is small at this energy. The asymmetry index is slightly dependent on the Lorentzian broadening $\Gamma$ since we have summed contributions from different layers with different $\alpha$ values. The index is about 2.6 that according to Eq. (20) corresponds to an effective $\alpha$ of about 0.3.

In the superconducting state the loss function should have a gap. We mimic this gap by using a rectangular alpha function

$$\alpha_{2D}(\omega)=\alpha_0\theta(\omega-\omega_{sc})\theta(\omega_0-\omega), \qquad (21)$$

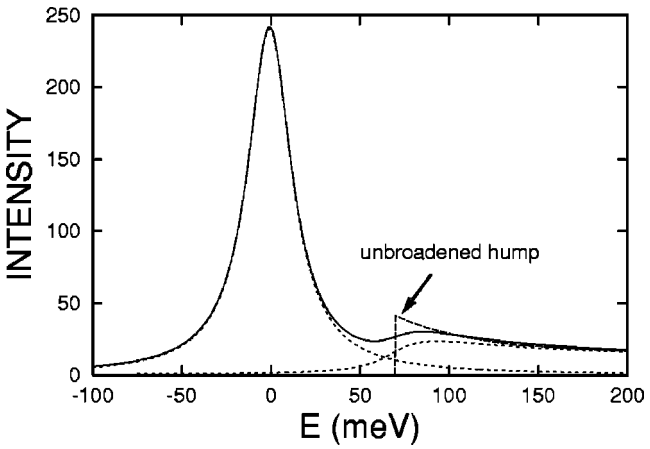


FIG. 10. The loss function $P_{\mathbf{k}}^{2D}$ for a gapped spectrum using the simple parametrization in Eq. (21). The Lorentzian broadening is $\Gamma=15$ meV.

using the same values for $\alpha_0$ and $\omega_0$ as in Fig. 8. For the gap $\omega_{sc}$ we take $\omega_{sc}=70$ meV. In Fig. 10 we show the corresponding $P_{\mathbf{k}}^{2D}(\omega)$ broadened with a Lorentzian of width $\Gamma=15$ meV. Our choice of parameters is only made to illustrate the qualitative behavior to be expected. The curve clearly shows the peak-dip-hump line shape found experimentally (for a recent reference see, e.g., Ref. 19).

Recently it has been possible to obtain very accurate tunneling data from Bi2212, and it is of interest to compare these data with the PES satellites,[20] since the tunneling data also show peak-dip-hump structures.[21] PES and tunneling are basically different spectroscopies. There can, however, be qualitative similarities since in both cases the electrons couple to 3D quasi-boson excitations such as phonons, electron-hole pairs, plasmons, magnons, etc. In our treatment of PES we take the states of a particular 2D layer as given and study the effect to low order of the sudden appearance of a hole in the 2D system on the quasi-bosons (intrinsic excitations) as well as of the coupling of the photoelectron leaving this layer to the quasi-bosons (extrinsic excitations), and their interference [cf. Eqs. (8)–(10), or equivalently Eq. (26) in Appendix A]. We found that the intrinsic contributions dominate for small excitation energies.

Tunneling is traditionally described by the spectral function that involves matrix elements of the electron annihilation operator between the initial state and the excited states.[22,23] The excited states consist of a 2D layer state with a hole, and some state of the quasi-bosons in the presence of a localized hole. In lowest-order perturbation theory the probability for a final state with excited quasi-bosons is given by the first term in Eq. (10). This means that *the intrinsic contribution to PES and the tunneling currents are the same except for* the mean free path effect in PES shown in Eq. (8), and the summation over momenta in tunneling (giving the density of states, DOS) contra momentum conservation from the dipole matrix element in PES. As mentioned above, we modify this analysis valid for the normal state, by simply assuming that the loss function should have a gap in the superconducting state.

In Bi2212 we have a van Hove singularity (VHS) at the

Fermi level, which makes the difference between DOS and momentum conservation of less importance (there might actually even be two VHS's if the two CuO planes 3 Å apart produce a significant splitting). More important is that in PES the electrons come from a thin surface region (of the order of the mean free path) while in tunneling they may come from an extended region that can be hundreds of angstroms, and that the coupling functions $V(z)$ are strongly $z$ dependent. Additionally, there are two energy gaps (superconducting gap and pseudogap), which further complicates the picture. There is thus no way that PES and tunneling structures can be quantitatively the same, but since the same quasi-bosons are involved, there may well be qualitative similarities even though the coupling strengths can be quite different. It should also be noted that we take the spectral function for the 2D system as a sharp peak (the function often calculated by theoreticians using say a $t$-$J$ model), and have no means to estimate the relative strengths of the true 2D spectral function relative to the loss structure analyzed here.

In our analysis we have only treated the plasmons for the simple reason that the experimental loss data at hand did not have resolution enough to show phonons and other low-energy excitations. If such $(q=0)$ data appear showing additional quasi-bosons one is faced with introducing reasonable dispersions, and finding reasonable extrapolations of the bulk coupling function to account for the presence of the surface.

## IV. CONCLUDING REMARKS

This paper is concerned with effects of external losses in photoemission, and the extent to which the commonly used sudden approximation works for strongly correlated layered materials. We have earlier found that for a strongly correlated *localized* system the sudden approximation is reached rather quickly, at about 10 eV.[1] For a weakly correlated system, on the other hand, like an $sp$-metal or semiconductor, the sudden limit is approached very slowly, on the keV scale.[5] The slow approach is connected with strong destructive interference between the intrinsic and extrinsic mechanisms for plasmon production. The cancellation is particularly strong for small-momentum plasmons where the long-wave plasmons are excited by the average potential from the core hole and photoelectron, which is zero.[24] The asymmetric line shape in core electron photoemission from metals is, on the other hand, hardly affected by the external loss processes.[5]

We are interested in energies where the sudden limit is reached for the strongly correlated layer from which the photoelectron comes, and derive an expression for photocurrent as a convolution of the sudden approximation for the current from the layer with an effective loss function, $P_{\mathbf{k}}(\omega)$ [Eq. (7)]. We assume, as far as the loss properties are concerned, that the photoelectron comes from a localized position. In our specific example, Bi2212, the $c$ value is 15.4 Å (neglecting crystallographic shear), and almost all contributions come from the first unit cell. The two first CuO layers are at $0.39c$ and $0.61c$ from the surface (which is between two BiO layers).[25] With a photon energy of 1 a.u. the maximum electron energy (inside the solid) is 1.15 a.u.$=31$ eV if we take the bandwidth as 0.15 a.u. Our energy loss calculations give $\lambda = 17.8a_0$ (Fig. 2). The $\exp(-z_0/\lambda)$ factor then is 0.53, 0.37, 0.10, and 0.07 for the first four CuO layers. We thus expect large photoemission contributions only from the first unit cell.

To obtain $P_{\mathbf{k}}(\omega)$ we use a previously developed method based on a quasi-boson model, where the electron-boson coupling is given by fluctuation potentials related to the dielectric response function.[15] We find that the energy loss function, which we take from experimental data, can be related to the screened potential that we need to calculate the (intrinsic and extrinsic) losses in photoemission. The fluctuation potentials related to the electrons in the layers are universal functions, which are easily calculated [Eqs. (11) and (12)]. They have some resemblance to a surface plasmon potential, but penetrate the whole solid and have the Bloch wave symmetry. We use the real part (or equivalently the imaginary part) of a phase-shifted bulk potential to get a potential that is zero at the surface, and mimics the potential we have in a finite solid. The fluctuation potential is integrated over $z$ together with a propagation function $f(z)$ [Eq. (10)] that takes the photoelectron out of the solid. This integral is in turn integrated with the loss function (taken from experiment), $\mathrm{Im}\,\varepsilon^{-1}(q,Q,\omega)$, to give functions $\alpha_{2D}(\omega)$ and $\alpha_{3D}(\omega)$ that are simply related to the effective loss function $P_{\mathbf{k}}(\omega)$ [Eq. (16)]. When we use plane waves instead of Bloch functions in the propagation function $f(z)$, all specific materials properties are embodied in the loss function. The propagation function has both an intrinsic and an extrinsic contribution that interfere.

From Eq. (16) we see that $P_{\mathbf{k}}(\omega)$ is scaled down with $z_0$, the distance of the layer from the surface, while the fluctuation potentials increase with $z$. The reason for that increase is that the boundary condition forces the fluctuation potential in the first unit cell to be much weaker than the bulk potential (cf. Figs. 3 and 4). The contributions to the $\alpha$ functions from excitations in different layers are shown in Fig. 5 for photoemission from different layers.

The mean free path is found to be considerably longer than obtained by Norman *et al.*,[4] about 12 Å rather than 3 Å, at say 20 eV (Fig. 2). Measurements by the ITR-2PP technique[26] give a lifetime of $\tau = 10$ fs at an energy $\varepsilon = 3$ eV above the Fermi surface. The mean free path is $\lambda = v\tau$. Converting energy to velocity by $mv^2/2 = \varepsilon$ gives a mean free path $\lambda = 103$ Å as compared to our result of about 17 Å at that energy. This is an indication that our values rather are on the low side. It is, however, hard to know what is the correct conversion between energy and velocity at such low energies, which makes a comparison very uncertain.

From Fig. 1 we see that the 2D losses occur only for small energies, at 5 eV the bulk losses take over. The 2D losses go to zero quite slowly, just like the bulk losses, but on another energy scale. If we only had 2D losses, the minimum mean free path would be long, about 20 Å. The general behavior of the 3D mean free path follows a well-known pattern. The mean free path has a minimum of about 5 Å at an energy of 3–4 times the energy where the loss function has its center

of gravity. We have used the Born approximation to evaluate the mean free paths. This may seem a very crude approximation at low energies. However, the Born scattering expression with a basis of Bloch waves and Bloch energies rather than plane waves and free electron energies agrees with the GW approximation, which is commonly used also at low energies. Further it was shown by Campillo *et al.*[7] that plane waves and free electron energies was not that bad, as long as the energies in the dielectric function are well approximated.

Our main concern is the behavior of the effective broadening function at small energies where it is dominated by the 2D losses. The 3D contributions set in at somewhat higher energies, and give a rather structureless contribution. What we here for convenience call 2D losses is of course actually also a 3D effect since it comes from excitations of a coupled set of 2D layers. To allow a qualitative discussion we represent the $\alpha_{2D}$ functions by a rectangular distribution. Looking at Fig. 5 this may seem rather crude, but Fig. 8 shows that the corresponding $P_{\mathbf{k}}(\omega)$ functions are not too different. The rectangular distribution allows an analytic solution [Eq. (19)] valid out to the cutoff $\omega_0(\omega_0 \simeq 0.1$ a.u.$\simeq 3$ eV). $P_{\mathbf{k}}(\omega)$ has only a fairly small tail beyond $\omega_0$. In Fig. 9 we plot the total $P_{\mathbf{k}}(\omega)$ function (sum over the four first layers, properly mean free path weighted), calculated with the rectangular approximation and broadened with Lorentzians of different widths. We note the marked asymmetry. The asymmetry is described by an index $\gamma_{as}$, defined in Eq. (20). When $P_k(\omega)$ derives from only one (rectangular) $\alpha$ function $\gamma_{as}$ is a function of the singularity index $\alpha_0$, $\gamma_{as}(\alpha_0)$. The index $\gamma_{as}$ is then independent of the amount of Lorentzian broadening $\Gamma$. If the $J_{2D}$ function has a power law singularity with singularity index $\alpha_L$, the asymmetry index contains the sum of the two indices, $\gamma_{as}(\alpha_0+\alpha_L)$.

In Fig. 7 we plot contributions to the loss function $P_k(\omega)$ from different layers. It is interesting that the first two layers give about the same contribution, while the contributions from the next two are tiny. In the left part of Fig. 6 we show the importance of the intrinsic contributions to $\alpha_{2D}$. The behavior here is thus similar to what was found previously for metals.[5] In the right part of Fig. 6 we show the approach to the bulk limit curves. This approach is very slow for $\alpha_{2D}$ while, like in metals, it is fast for $\alpha_{3D}$. The slow approach for $\alpha_{2D}$ of course comes from the slow approach to the bulk limit of the 2D fluctuation potentials (Fig. 4).

In a paper by Liu, Anderson, and Allen from 1991,[27] they discussed the line shapes of $Bi_2Sr_2BaCu_2O_8$ along the $\Gamma$-$X$ direction obtained by Olson *et al.*[28] for 22 eV photons. They concluded that neither the Fermi liquid nor the marginal Fermi liquid theories could fit the slow falloff of the spectrum at higher energies. Our results offer a possibility that the slow falloff may be due to intrinsic creation of acoustic plasmons in a coupled set of CuO layers, an effect not present if only one CuO layer is considered. This broadening is mostly intrinsic, i.e., if we treat a 3D system we have an almost intrinsic effect. However, most theoretical discussions concern an isolated 2D system, compared to which we find an appreciable extra broadening from the coupling between the layers.

The PES spectra change strongly when we go to the superconducting state. The main peak sharpens and a peak-dip-hump structure develops. This effect has been interpreted as a coupling of the 2D state to the $(\pi,\pi)$ collective mode.[19] Here we find that this effect also can arise from the gapping of the loss function caused by the lack of low energy excitations in a superconductor as shown in Fig. 10. Without a more accurate model we find it difficult to decide which is the correct explanation, possibly it could be a combination of both mechanisms. Since the gapping of the loss function is related to the superconducting gap, also with our mechanism the hump will scale with the gap. It is clear that the experimental peak-dip-hump structure rides on a background that is not predicted by our expressions, nor by anyone else's. Our theory is however rather schematic with its strict separation of a 2D and a 3D part, while in reality the bands are hybridized. If we extend our approach to a more detailed treatment of the underlying bandstructure, the background could well be strongly changed. Such an extension represents a very large numerical task but with the present pilot treatment we can at least start thinking seriously about the difficult background problems in photoemission.

In recent papers Joynt *et al.*[3] discussed a broadening mechanism due to the interaction between the photoelectron when outside the solid and the electrons in the solid. This is a different mechanism than in this paper, which adds additional broadening. Their discussion only involved the energy loss part and not the elastic contribution and can thus not be directly compared to experiment. We hence find their claims regarding pseudogaps uncertain.

It should be stressed that we cannot claim any high quantitative accuracy. We have put in dispersion in the loss function using a crude approximation. Since, however, dispersion is very important we think our predictions are substantially better than if dispersion had been neglected. We have only considered normal emission where the electrons come from the $\Gamma$ point, while the interesting experiments concern electrons from the Fermi surface. However, there is no reason that the effective loss function should change qualitatively when we go away from normal emission. The behavior of the loss function when $\omega \rightarrow 0$ has been disputed. Most authors seem to believe the approach is linear, but there are also claims that it should be quadratic.[29] If it were quadratic, the corresponding $\alpha$ function would start linearly rather than with a constant. However, $\alpha(\omega)$ would have to rise very fast to reproduce the behavior of the loss function for the (quite small) energies where it is known to be approximately linear. Thus the pure power-law behavior of $P_k(\omega)$ would be lost, but Lorentzian broadened curves would probably not differ much. Our fluctuation potentials are obtained by phase-shifting bulk potentials to make them zero at the surface, and define them as zero outside the solid. This procedure turned out to be fairly good in the metallic case, where we could check with more accurately calculated fluctuation potentials. Again this approximation is crude, but we believe it to be fundamentally better than if we had used a step function on the bulk potential. Since the phase of the bulk potential is arbitrary, such a procedure would anyhow have been arbitrary. To calculate more accurate potentials is a very large numerical undertaking.

One may also question the use of a bulk expression to estimate of the mean free path at the fairly low energies that we are concerned with, after all we found strong effects when modifying the fluctuation potentials for surface effects. It does not seem easy to make a strong statement here, and we can only refer to ''the state of the art,'' that bulk mean free paths are successfully used in low-energy electron diffraction and also in low-energy lifetime calculations that are compared with time-resolved two-photon PES (TR-2PPE) experiments.[30]


## ACKNOWLEDGMENTS

We thank J.W. Allen, J.C. Campuzano, A. Fujimori, A.J. Millis, M.R. Norman, and Z.-X. Shen for constructive and informative comments. One of the authors (J.D.L.) acknowledges the fellowship from the Japan Society for the Promotion of Science.


## APPENDIX A: DERIVATION OF THE PHOTOCURRENT EXPRESSION

We will here derive Eq. (7). The 2D and 3D parts in Eq. (5) factor,

$$\tau(\mathbf{k},s_1,s_2)=\sum_i \langle N_{2D}-1,s_2|c_i|N_{2D}\rangle \tau^{3D}(\mathbf{k},s_1,i),$$

where

$$\tau^{3D}(\mathbf{k},s_1,i) \equiv \langle \mathbf{k}|\langle N_B^*,s_1| \times\left[1+V\frac{1}{E(N_B^*,s_1)+\varepsilon_{\mathbf{k}}-H_{QB}-h-V}\right]|N_B\rangle\Delta|i\rangle.$$

We note that $\langle N_{2D}-1,s_2|c_i|N_{2D}\rangle$ is the basic part in the spectral function for the 2D system, and that the 2D and 3D parts are entangled through the index $i$. We have used Eq. (6) to eliminate the index $s_2$, $E-E(N_{2D}-1,s_2)=E(N_B^*,s_1)+\varepsilon_{\mathbf{k}}$.

Expanding to first order in $V$ we have,[31]

$$\tau^{3D}(\mathbf{k},s,i)=-\frac{V_h^s}{\omega_s}\langle \mathbf{k}|\Delta|i\rangle+\langle \mathbf{k}|V^s\frac{1}{\omega_s+\varepsilon_{\mathbf{k}}-h-\Sigma}\Delta|i\rangle, \tag{A1}$$

where $\Sigma$ is the self energy coming from a summation to infinite order in $V$, and we have used the relations

$$\langle N_B^*,s|N_B\rangle=-\frac{V_h^s}{\omega_s},\quad E(N_B^*,s)=\omega_s,$$

$$\langle N_B^*,s|V|N_B\rangle=V^s(\mathbf{r}).$$

The energy argument of $\Sigma$ is $\omega_s+\varepsilon_{\mathbf{k}}$.

These results are only meaningful when $\omega_s\neq 0$. For the moment we take the excitation spectrum to have a gap, $\omega_s>\omega_0$, for all $s$ except $s=0$. For $s=0$ we have

$$|\langle N_B^*,0|N_B\rangle|^2=e^{-a},\quad a=\sum_s\left|\frac{V_h^s}{\omega_s}\right|^2.$$

Also the $s\neq 0$ terms in Eq. (A1) have the $\exp(-a/2)$ factor, when we go beyond first order in $V$.

We use plane waves for the parallel components of the fluctuation potential, $V^s(\mathbf{r})=e^{i\mathbf{QR}}V(q_z,\mathbf{Q},z)$. Neglecting the reflected component, we similarly write the photoelectron wave function as $\psi_{\mathbf{k}}(\mathbf{r})=e^{i\mathbf{KR}}\psi_{k_z}^{1D}(\mathbf{K},z)$. We further replace $\mathrm{Im}\,\Sigma$ by $-i\Gamma$, and absorb $\mathrm{Re}\,\Sigma$ in $h$. The photoelectron energy is $\varepsilon_{\mathbf{k}}=(\mathbf{K}^2+k_z^2)/2$. We can now simplify the last term in Eq. (A1) (cf. Ref. 5) to become,

$${}^{PW}\langle \mathbf{K}-\mathbf{Q}|\langle \psi_{k_z}^{1D}|V(q_z,\mathbf{Q},z) \times\frac{1}{\kappa^2/2-t_z-[V_{cryst}(z)-V_0]}\Delta|i\rangle,$$

where

$$\frac{\kappa^2}{2}=\omega_s+\varepsilon_{\mathbf{k}}-\frac{(\mathbf{K}-\mathbf{Q})^2}{2}-V_0+i\Gamma_1, \tag{A2}$$

$$\Gamma_1=-\mathrm{Im}\,\Sigma^0(k_1,k_1^2/2),\quad k_1^2/2=\omega_s+\varepsilon_{\mathbf{k}}-V_0,$$

$$t_z=-\frac{1}{2}\frac{\partial^2}{\partial z^2}.$$

${}^{PW}\langle \mathbf{K}-\mathbf{Q}|$ is a plane wave 2D function, we have neglected the variation of the crystal potential in the lateral directions, the inner potential $V_0$ is some average of $V_{cryst}$, and $\Sigma^0(k,\omega)$ is the electron gas self-energy. For the 1D Green's function we have approximately (see Appendix C),

$$\langle z|\frac{1}{\kappa^2/2-t_z-[V_{cryst}(z)-V_0]}|z'\rangle=A\psi_\kappa^<(z_<)\psi_\kappa^>(z_>).$$

Here $\psi_\kappa^<$ and $\psi_\kappa^>$ are damped Bloch functions, $\psi_\kappa^<$ decreasing towards the surface, and $\psi_\kappa^>$ decreasing towards the inner of the crystal (the crystal is on the positive half of the $z$ axis), $z_>=\max(z,z')$, $z_<=\min(z,z')$, and the coefficient $A$ is roughly $A=(i\kappa)^{-1}$. In our calculations we will use the simplest possible approximation $\psi_\kappa^>(z)=\exp(i\kappa z)$, and $\psi_\kappa^<(z)=\exp(-i\kappa z)$.

The $z$ part of the photoelectron wave function is $[\psi_{\tilde{k}_z}^>(z)]^*$, with

$$\frac{\tilde{k}_z^2}{2}=\frac{k_z^2}{2}-V_0+i\Gamma_2,\quad \Gamma_2=-\mathrm{Im}\,\Sigma^0(k_2,k_2^2/2),$$

$$k_2^2/2=\varepsilon_{\mathbf{k}}-V_0. \tag{A3}$$

We note that $\Gamma_1$ and $\Gamma_2$ are different.

We give a few comments on the relation between the electron energy inside the solid and outside. $V_{cryst}(z)$ is defined as $V_{cryst}=V_H+\mathrm{Re}\,\Sigma(\omega)+\phi^{DP}$, where $\phi^{DP}$ is the dipole contribution to the work function $\phi$, with $\phi$ defined as negative. For the argument $\varepsilon$ in $\mathrm{Im}\,\Sigma(\varepsilon)$ we should choose

the eigenvalue in the quasiparticle equation $[t+V_{cryst}(\mathbf{r})-\varepsilon_{\mathbf{k}}]\psi_{\mathbf{k}}(\mathbf{r})=0$. For an electron gas this gives $V_{cryst}=\mathrm{Re}\,\Sigma^0(k,\varepsilon_k)+\phi^{DP}$ since $V_H=0$. The work function is by definition $\phi=\varepsilon_F+\mathrm{Re}\,\Sigma^0(k_F,\varepsilon_{k_F})+\phi^{DP}$. Since $\mathrm{Re}\,\Sigma^0(k,\varepsilon_k)$ varies fairly slowly with $k$ out to about $2k_F$, we can take $V_0=\phi-\varepsilon_F=-|\phi|-\varepsilon_F$. When we leave the electron gas a reasonable definition for $V_0$ is $V_0=-|\phi|-W$, where $W>0$ is the bandwidth. The maximum kinetic energy the photoelectron can have outside the solid is, by energy conservation, $\omega_{phot}-|\phi|$, corresponding to the energy $\omega_{phot}+W$ inside the solid. In our calculations we have taken $|\phi|=W=0.15$ a.u. Errors in this choice have a minor effect, and the relative error decreases with increasing photon energy. All calculations are made for a photon energy of 1 a.u.

We consider only forward propagation for the Green's function from the excited layer to the surface (cf. Ref. 32), and have,

$$\tau^{3D}(\mathbf{k},s,i)=-\frac{V_h^s}{\omega_s}\langle\mathbf{k}|\Delta|i\rangle + \frac{1}{i\kappa}\int_0^\infty \psi^{>}_{\tilde{k}_z}(z')V(q_z,\mathbf{Q},z')\psi^{<}_{\kappa}(z')dz' \times\int_{z'}^\infty dz''\psi^{>}_{\kappa}(z'')\int d\mathbf{R}e^{-i(\mathbf{K}-\mathbf{Q})\mathbf{R}}\Delta(\mathbf{R},z'') \times\psi_i(\mathbf{R},z''),$$

or

$$\tau^{3D}(\mathbf{k},s,i)=-\frac{V_h^s}{\omega_s}\langle k_z,\mathbf{K}|\Delta|i\rangle + \frac{1}{i\kappa}\int_0^{z_0} dz\,\psi^{>}_{\tilde{k}_z}(z)V(q_z,\mathbf{Q},z)\psi^{<}_{\kappa}(z) \times\langle\kappa,\mathbf{K}-\mathbf{Q}|\Delta|i\rangle.$$

If we approximate the $\psi$ functions with plane waves the dipole matrix elements $\langle\tilde{k}_z,\mathbf{K}|\Delta|i\rangle$ and $\langle\kappa,\mathbf{K}-\mathbf{Q}|\Delta|i\rangle$ depend on the position of the excited layer through the factors $\exp(i\tilde{k}_z z_0)$ and $\exp(i\kappa z_0)$. We note that the electron lifetime is $\tau=1/(2\Gamma)$ and from Eq. (A3) we have $2\,\mathrm{Im}\,\tilde{k}_z\simeq 2\Gamma_2/|\tilde{k}_z|=1/\lambda$ where $\lambda=v\tau$ is the mean free path. Neglecting the recoil momentum $\mathbf{Q}$ picked up by the quasi-boson "$s$" the entanglement between the 2D and 3D parts disappears and we have the intuitively expected result,

$$J_{\mathbf{k}}(z_0,\omega_{phot})=\int J^{2D}_{\mathbf{k}}(z_0,\omega)P_{\mathbf{k}}(z_0,\omega_{phot}-\omega)d\omega, \tag{A4}$$

with

$$J^{2D}_{\mathbf{k}}(z_0,\omega)=\sum_{s_2}\left|\sum_i\langle N_{2D}-1,s_2|c_i|N_{2D}\rangle\langle k,\mathbf{K}|\Delta|i\rangle\right|^2 \times\delta(\omega+E_{s_2}-\varepsilon_{\mathbf{k}}),$$

$$P_{\mathbf{k}}(z_0,\omega)=e^{-z_0/\lambda-a}\left(\delta(\omega)+\sum_s\left|-\frac{V_h^s}{\omega_s}+\frac{e^{i(\kappa-\tilde{k}_z)z_0}}{i\kappa} \times\int_0^{z_0}dz e^{i(\tilde{k}_z-\kappa)z}V(q_z,\mathbf{Q},z)\right|^2\delta(\omega-\omega_s)\right), \tag{A5}$$

where $s=(q_z,\mathbf{Q})$. We have included the $s=0$ term and the common factor $\exp(-a)$. *The photocurrent $J_{\mathbf{k}}(z_0,\omega_{phot})$ thus is a convolution between the sudden approximation 2D current $J^{2D}_{\mathbf{k}}(z_0,\omega)$, and an effective loss function $P_{\mathbf{k}}(z_0,\omega)$.*

## APPENDIX B: DIELECTRIC RESPONSE

Dielectric response is usually treated in the random-phase approximation (RPA), and RPA has indeed proved extremely useful in many cases.[33] For, e.g., high-$T_c$ materials RPA may, however, not be good enough, and we will derive formal expressions without resorting to RPA. These expressions allow us to connect the energy loss results to the screened potentials needed to discuss photoemission. The energy loss data are then taken from experiment. Some of our results can be found in Griffin's classic paper,[34] but not those that are crucial to our treatment.

The response functions $\chi^0$, $\chi$, and $\varepsilon^{-1}$ are defined from (in a schematic notation)

$$\rho^{ind}=\chi^0V^{tot}=\chi V^{ext},\quad V^{tot}=v\rho^{ind}+V^{ext}=\varepsilon^{-1}V^{ext}.$$

This leads to the relations

$$\varepsilon^{-1}=1+v\chi,\quad \chi=\chi^0+\chi^0v\chi.$$

Since $\rho^{ind}$ and $V^{ext}$ are exactly defined, no approximations are involved in the definitions of $\chi^0$, $\chi$, and $\varepsilon^{-1}$.

We now specialize to two layers per unit cell. We choose the origin of the $z$ coordinate at the center of the cell such that we have two layers at $z=\pm d$. We write the response functions as

$$\chi^0(\mathbf{r},\mathbf{r}')=\sum_m\sum_n^{\pm1}w(z-cm-dn)w(z'-cm-dn) \times\tilde{\chi}^0(\mathbf{R}-\mathbf{R}'),$$

$$\chi(\mathbf{r},\mathbf{r}')=\sum_{mm'}\sum_{nn'}^{\pm1}w(z-cm-dn)w(z'-cm'-dn') \times\tilde{\chi}_{nn'}(m-m';\mathbf{R}-\mathbf{R}').$$

We have assumed translational invariance in the layers, and that there are no transverse excitations, i.e., that the electrons always stay in the lowest transverse state $\phi_0(z)$, $w(z)=|\phi_0(z)|^2$. We have taken the overlap between $w(z)$ and $w(z+c)$ as zero, and neglected interlayer coupling in $\chi^0$. This latter neglect probably has no effect. Interlayer coupling in $\chi^0$ is absent in any one electron theory with a local potential, and thus, e.g., in RPA. It is also absent in the static ($\omega$

$=0$) case since this case can be described by density functional theory transform where the potential is local.

We Fourier transform with respect to **R**, and separate into contributions from different layers

$$\chi^0(z,z';\mathbf{Q})=\sum_n \chi_n^0(z,z';\mathbf{Q}),$$

$$\chi(z,z';\mathbf{Q})=\sum_{nn'} \chi_{nn'}(z,z';\mathbf{Q}), \tag{B1}$$

where

$$\chi_n^0(z,z';\mathbf{Q})=\sum_m w(z-cm-dn)w(z'-cm-dn)\tilde{\chi}^0(\mathbf{Q}),$$

$$\chi_{nn'}(z,z';\mathbf{Q})=\sum_{mm'} w(z-cm-dn)w(z'-cm'-dn') \times\tilde{\chi}_{nn'}(m-m';\mathbf{Q}).$$

The integral equation $\chi=\chi^0+\chi^0 v\chi$ can be written as (suppressing the **Q** variable),

$$\chi_{nn'}(z,z')=\chi_n^0(z,z')\delta_{nn'} +\sum_{n''}\int \chi_n^0(z,z_1)v(z_1,z_2)\chi_{n''n'}(z_2,z')dz_1dz_2. \tag{B2}$$

This is the same result as in Eq. (1) in Griffin's paper.[34]

We Fourier transform $\chi_n^0(z,z')$ with respect to $z$ and $z'$, using discrete $q_z$ values and the orthonormal set $\{L^{-1/2}\exp(iq_z z)\}$

$$\chi_n^0(q_z,q_z')=\frac{1}{c}w(q_z)w(q_z')\tilde{\chi}^0 e^{i(q_z-q_z')dn},$$

where it is understood that $q_z$ and $q_z'$ differ by a reciprocal lattice vector $G$, $L$ is the length of the sample, and $c$ the lattice constant. Similarly we have for $\chi_{nn'}(q_z,q_z')$

$$\chi_{nn'}(q_z,q_z')=\frac{1}{c}w(q_z)w(q_z')\tilde{\chi}_{nn'}(q_z)e^{iq_z dn}e^{-iq_z' dn'}, \tag{B3}$$

where

$$\tilde{\chi}_{nn'}(q_z)=\sum_m \tilde{\chi}_{nn'}(m-m')e^{iq_z c(m-m')}.$$

We note that $\tilde{\chi}_{nn'}(q_z)$ is a periodic function in $q_z$, $\tilde{\chi}_{nn'}(q_z)=\tilde{\chi}_{nn'}(q_z+G)$. Equations (B1) and (B3) give

$$\chi(q_z,q_z')=\frac{1}{c}w(q_z)w(q_z')\sum_{nn'}\tilde{\chi}_{nn'}(q_z)e^{iq_z dn}e^{-iq_z' dn'}. \tag{B4}$$

We can separate out the $w$ factors in Eq. (B2) to obtain an equation for $\tilde{\chi}_{nn'}(q_z)$

$$\tilde{\chi}_{nn'}(q_z)=\tilde{\chi}^0_{nn'}+\frac{1}{c}\sum_{n_1n_2}\tilde{\chi}^0_{nn_1}\tilde{V}_{n_1n_2}(q_z)\tilde{\chi}_{n_2n'}(q_z), \tag{B5}$$

where $\tilde{\chi}^0_{nn'}=\tilde{\chi}^0\delta_{nn'}$ and $\tilde{V}$ is a $2\times2$ matrix periodic in $q_z$,

$$\tilde{V}_{nn'}(q_z)=\sum_G v(q_z+G)w^2(q_z+G) \times\exp[-i(q_z+G)d(n-n')].$$

Equation (B5) gives the matrix solution

$$\tilde{\chi}_{nn'}(q_z)=\left[\tilde{\chi}^0\frac{1}{1-\tilde{V}(q_z)\tilde{\chi}^0/c}\right]_{nn'}.$$

We write

$$\tilde{V}_{nn'}(q_z)=\begin{pmatrix} V_0(q_z) & V_1(q_z)e^{i\phi(q_z)} \\ V_1(q_z)e^{-i\phi(q_z)} & V_0(q_z)\end{pmatrix},$$

where

$$V_0(q_z)=\tilde{V}_{1,1}(q_z)=\sum_G v(q_z+G)w^2(q_z+G),$$

$$V_1(q_z)=|\tilde{V}_{1,-1}(q_z)|,$$

and have

$$\tilde{\chi}_{nn'}(q_z)=\frac{1}{2}\begin{pmatrix} \chi_1+\chi_2 & (\chi_1-\chi_2)\exp(i\phi) \\ (\chi_1-\chi_2)\exp(-i\phi) & \chi_1+\chi_2\end{pmatrix},$$

$$\chi_1=\frac{\tilde{\chi}^0}{1-(\tilde{\chi}^0/c)(V_0+V_1)},\quad \chi_2=\frac{\tilde{\chi}^0}{1-(\tilde{\chi}^0/c)(V_0-V_1)}.$$

Here $\chi_1$ and $\chi_2$ are functions of $q_z$, **Q**, and $\boldsymbol{\omega}$. From Eq. (B4) the energy loss function becomes

$$v(q_z,\mathbf{Q})\mathrm{Im}\,\chi(q_z,q_z;\mathbf{Q},\boldsymbol{\omega}) =\frac{v(q_z,\mathbf{Q})w^2(q_z)}{c}\mathrm{Im}[\chi_1+\chi_2+(\chi_1-\chi_2) \times\cos\{2q_z d+\phi(q_z,\mathbf{Q})\}],$$

to be compared with the screened potential $\mathrm{Im}\,W=v(\mathrm{Im}\,\chi)v$. From Eqs. (B1) and (B3) we have

$$\mathrm{Im}\,W(\mathbf{Q},\omega;z,z')=\mathrm{Im}\sum_{nn'}^{\pm1}\frac{1}{2\pi}\int_{-\pi/c}^{\pi/c}V(\mathbf{Q},q_z,z-dn) \times\frac{\tilde{\chi}_{nn'}(\mathbf{Q},\omega,q_z)}{c}V^*(\mathbf{Q},q_z,z'-dn')dq_z, \tag{B6}$$

where

$$V(Q,q_z,z)=\sum_G v(q_z+G,Q)w(q_z+G)e^{-i(q_z+G)z}. \tag{B7}$$

There is thus no simple relation between $\mathrm{Im}\,W(z,z')$ and the loss function unless the non-diagonal elements in $\tilde{\chi}_{nn'}(q_z)$ can be neglected. For typical values of $q_z$ and $Q$ it, however, turns out that $V_1/V_0$ is 0.2–0.3. Taking $\chi_1=\chi_2$ and using the symmetries $V(q_z,-z)=V(-q_z,z)=V^*(q_z,z)$ and $\chi_n(q_z)=\chi_n(-q_z)$ we can write Eq. (B6) as

$$\mathrm{Im}\,W(z,z')=\sum_{i=1}^{2}\sum_{n}^{\pm 1}\frac{1}{\pi}\int_0^{\pi/c}V_i(q_z,z-dn)\times\frac{\mathrm{Im}\,\chi_0(q_z)}{c}V_i(q_z,z'-dn)dq_z,$$

where $V_1$ is the real and $V_2$ the imaginary part of $V(q_z,z)$ and $\chi_0=(\chi_1+\chi_2)/2$. The real and imaginary parts turn out to give equal contributions to $\mathrm{Im}\,W$.

So far we have results for a set of coupled layers sitting in vacuum. We can take account of the embedding electrons (the 3D bulk excitations in our parametrization) by using

$$\chi^0(z,z';\mathbf{Q})=\chi_b^0(z-z';\mathbf{Q})+\sum_m w(z-cm)\times w(z'-cm)\tilde{\chi}_2^0(\mathbf{Q}). \tag{B8}$$

This leads to a 3D bulk contribution in $\mathrm{Im}\,W(z,z')$, and to screening of the 2D susceptibility $\chi$. The same screening, however, appears also in the loss function, so we can forget about it in our problem. We note that the bulk screened potential can be anisotropic since $\chi_b^0(q_z,\mathbf{Q})$ can depend on both $q_z$ and $\mathbf{Q}$, and not only on $q^2=q_z^2+\mathbf{Q}^2$.

We derived the relation between $\chi$ and $\chi^0$ by solving the integral equation $\chi=\chi^0+\chi^0 v\chi$. This equation can be written as $\chi=\chi_{2D}+\chi_{2D}v_{3D}\chi$, where $\chi_{2D}=\chi^0+\chi^0 v_{2D}\chi_{2D}$. Here $v_{3D}$ contains no intralayer parts, while $v_{2D}$ only has intralayer contributions. Since $\chi_{2D}$ is available from many sophisticated theoretical calculations, it is interesting to have the relation between $\chi^0=\chi_{2D}^0$ and $\chi_{2D}$. We write

$$\chi_{2D}(z,z')=w(z)w(z')\tilde{\chi}_{2D},$$

$$\chi_{2D}^0(z,z')=w(z)w(z')\tilde{\chi}_{2D}^0.$$

The equation $\chi_{2D}=\chi^0+\chi^0 v_{2D}\chi_{2D}$ gives, $\tilde{\chi}_{2D}=\tilde{\chi}_{2D}^0+\tilde{\chi}_{2D}^0 W_{00}\tilde{\chi}_{2D}$, where $W_{00}=\int w(z_1)v(z_1-z_2;\mathbf{Q})w(z_2)dz_1dz_2$. The desired relation is,

$$\tilde{\chi}_{2D}^0=\frac{\tilde{\chi}_{2D}}{1+W_{00}\tilde{\chi}_{2D}}.$$

## APPENDIX C: ON GREEN'S FUNCTIONS WHEN THE POTENTIAL IS COMPLEX

Green's function theory is usually developed using a real potential. Here we will shortly summarize the changes from having a complex potential. With a constant complex potential the equation ($\mathrm{Im}\,\kappa>0$),

$$\frac{1}{2}\left(\kappa^2+\frac{d^2}{dz^2}\right)G(z,z';\kappa)=\delta(z-z'),$$

has the solution (as is easily verified by direct substitution),

$$G(z,z';\kappa)=\frac{1}{i\kappa}e^{i\kappa|z-z'|}.$$

With $\kappa$ a function of $z$ the solution has the form,

$$G(z,z';\kappa)=wg_-(z_<)g_+(z_>),$$

where $w$ is a constant (cf., e.g., Arfken[35]),

$$w=\frac{2}{g_-(z)g_+'(z)-g_-'(z)g_+(z)}.$$

The boundary conditions are $g_-(z)\to 0$ for $z\to-\infty$ and $g_+(z)\to 0$ for $z\to\infty$.

In a slightly more general situation

$$\kappa(z)=\begin{cases}\kappa_1, z<0\\ \kappa_2, z>0\end{cases},\quad \mathrm{Im}\,\kappa_i>0,$$

we have

$$g_-(z)=e^{-i\kappa_1 z}\theta(-z)+(a_-e^{i\kappa_2 z}+b_-e^{-i\kappa_2 z})\theta(z),$$

$$g_+(z)=e^{i\kappa_2 z}\theta(z)+(a_+e^{i\kappa_1 z}+b_+e^{-i\kappa_1 z})\theta(-z),$$

$$a_-=\frac{1}{2}\left(1-\frac{\kappa_1}{\kappa_2}\right),\quad b_-=\frac{1}{2}\left(1+\frac{\kappa_1}{\kappa_2}\right),$$

$$a_+=\frac{1}{2}\left(1+\frac{\kappa_2}{\kappa_1}\right),\quad b_+=\frac{1}{2}\left(1-\frac{\kappa_2}{\kappa_1}\right),$$

$$w=\frac{2}{i(\kappa_1+\kappa_2)}.$$

For high energies $\kappa_1\simeq\kappa_2$ and the results reduce to those of the first model with $\kappa=$constant.

Finally we consider a model with,

$$\kappa(z)=\begin{cases}\kappa_1, z<0\\ \kappa_2(z), z>0\end{cases},\quad \mathrm{Im}\,\kappa_i>0,$$

$$g_-(z)=e^{-i\kappa_1 z}\theta(-z)+[a_-\psi_\kappa^>(z)+b_-\psi_\kappa^<(z)]\theta(z),$$

$$g_+(z)=\psi_\kappa^>(z)\,\theta(z)+(a_+e^{i\kappa_1 z}+b_+e^{-i\kappa_1 z})\theta(-z).$$

To see the difference between $\psi_\kappa^<(z)$ and $\psi_\kappa^>(z)$ we use the WKB approximation for the case $z>0$,

$$\psi_\kappa^>(z)\sim\exp\left[i\int_0^z\kappa_2(z')dz'\right],$$

$$\psi_\kappa^<(z)\sim\exp\left[-i\int_0^z\kappa_2(z')dz'\right].$$

Since $\kappa_2(z)$ is complex, the two solutions are basically different, not just complex conjugates. For higher energies and $z>0$ we have $g_-(z)\simeq\psi_\kappa^<(z), g_+(z)=\psi_\kappa^>(z)$.

[1] J.D. Lee, O. Gunnarsson, and L. Hedin, Phys. Rev. B **60**, 8034 (1999).
[2] J.D. Lee, Phys. Rev. B **61**, 8062 (2000).
[3] R. Joynt, Science **284**, 777 (1999); R. Haslinger and R. Joynt, J. Electron. Spectrosc. Relat. Phenom. **117-118**, 31 (2001).
[4] M.R. Norman, M. Randeria, H. Ding, and J.C. Campuzano, Phys. Rev. B **59**, 11 191 (1999).
[5] L. Hedin, J. Michiels, and J. Inglesfield, Phys. Rev. B **58**, 15 565 (1998).
[6] N. Nücker, H. Romberg, S. Nakai, B. Scheerer, J. Fink, Y.F. Yan, and Z.X. Zhao, Phys. Rev. B **39**, 12 379 (1989).
[7] I. Campillo, J.M. Pitarke, A. Rubio, E. Zarate, and P.M. Echenique, Phys. Rev. Lett. **83**, 2230 (1999).
[8] R.H. Ritchie and A. Howie, Philos. Mag. **36**, 463 (1977).
[9] S. Tougaard and B. Jörgensen, Surf. Sci. **143**, 482 (1984).
[10] N. Nücker, U. Eckern, J. Fink, and P. Müller, Phys. Rev. B **44**, 7155 (1991).
[11] H.-J. Hagemann, W. Gudat, and C. Kunz, J. Opt. Soc. Am. **65**, 742 (1975).
[12] C.J. Powell and A. Jablonski, J. Phys. Chem. Ref. Data **28**, 19 (1999).
[13] P. Hawrylak, G. Eliasson, and J.J. Quinn, Phys. Rev. B **37**, 10 187 (1988).
[14] F. Aryasetiawan, L. Hedin, and K. Karlsson, Phys. Rev. Lett. **77**, 2268 (1996).
[15] L. Hedin, J. Phys.: Condens. Matter **11**, R489 (1999).
[16] D.R. Harshman and A.P. Mills, Jr., Phys. Rev. B **45**, 10 684 (1992).
[17] C.-O. Almbladh and L. Hedin, in *Handbook on Synchr Rad*, edited by E. E. Koch (North-Holland, Amsterdam, 1983), Vol. 1.
[18] S. Doniach and M.J. Sunjic, J. Phys. C **3**, 28 (1970).
[19] J.C. Campuzano, H. Ding, M.R. Norman, H.M. Fretwell, M. Randeria, A. Kaminski, J. Mesot, T. Takeuchi, T. Sato, T. Yokoya, T. Takahashi, T. Moshiku, K. Kadowaki, P. Guptasarma, D.G. Hinks, Z. Konstantinovic, Z.Z. Li, and H. Raffy, Phys. Rev. Lett. **83**, 3709 (1999).
[20] We are indebted to Drs Z. X. Shen and A. Yurgens for providing informative viewpoints and unpublished background data. We are also grateful to the referee for prompting us to discuss tunneling.
[21] A. Yurgens, D. Winkler, T. Claeson, S.-J. Hwang, and J.-H. Choy, Int. J. Mod. Phys. B **13**, 3758 (1999), and paper presented at the APS March Meeting Seattle 2001.
[22] J.R. Schrieffer, D.J. Scalapino, and J.W. Wilkins, Phys. Rev. Lett. **10**, 336 (1963).
[23] G. D. Mahan, *Many-Particle Physics* (Plenum Press, New York, 1981), Sec. 9.3.
[24] J.W. Gadzuk, J. Electron Spectrosc. **11**, 355 (1977).
[25] T. Takahashi, H. Matsuyama, H. Katayama-Yoshida, Y. Okabe, S. Hosoya, K. Seki, H. Fujimoto, M. Sato, and H. Inokuchi, Phys. Rev. B **39**, 6636 (1989).
[26] W. Nessler, S. Ogawa, H. Nagano, H. Petek, J. Shimoyama, Y. Nakayama, and K. Kishio, Phys. Rev. Lett. **81**, 4480 (1998).
[27] L.Z. Liu, R.O. Anderson, and J.W. Allen, J. Phys. Chem. Solids **52**, 1473 (1991).
[28] C.G. Olson *et al.*, Phys. Rev. B **42**, 381 (1990).
[29] I. Bozovic, Phys. Rev. B **42**, 1969 (1990).
[30] P.M. Echenique, J.M. Pitarke, E.V. Chulkov, and A. Rubio, Chem. Phys. **251**, 1 (2000).
[31] We should have expanded $|N_B\rangle$ in eigenstates $|N_B^*,s\rangle$ of $H_{QB}$ $(P_h=1)$, which, e.g., would have given $h'=h-V_h$ instead of $h$ in the denominator (Ref. 5). In our approximate calculations we will, however, anyhow use simple plane waves as the eigenfunctions to $h'$.
[32] W. Bardyszewski and L. Hedin, Phys. Scr. **32**, 439 (1985).
[33] S.Y. Savrasov, Phys. Rev. B **54**, 16 470 (1996).
[34] A. Griffin, Phys. Rev. B **38**, 8900 (1988).
[35] G. Arfken, *Mathematical Methods for Physicists* (Academic Press, New York, 1985), pp. 898–901.